Advanced Fiber Materials
https://doi.org/10.1007/s42765-026-00692-4

REVIEW

Electrospun MOFs/Polymer Nanofiber Electrolytes for Solid-State Lithium Batteries: Interface Engineering and Synergistic Ion Transport

Xuemeng Gan[1] · Liangjie Gu[1] · Panpan Dong[1] · Xiahui Zhang[2] · Xingxing Jiao[1] · Guilin Feng[1] · Chunliu Xu[1] · Shihai You[1] · Junchao Zheng[2] · Min-Kyu Song[3] · Weiqing Yang[1]

Received: 30 October 2025 / Accepted: 24 January 2026

Abstract

Solid composite electrolytes that integrate metal–organic frameworks (MOFs) with polymer electrolytes combine the flexibility of polymers with structural order and rigidity of MOFs, emerging as promising candidates for high-performance solid-state lithium batteries. However, conventional physical blending leads to poor interfacial compatibility between MOFs and polymer, hindering ion transport and resulting in phase separation during processing and operation, thereby compromising structural integrity and compositional homogeneity. Electrospinning has recently offered an effective strategy to better incorporate MOFs within polymer matrices, enabling more uniform composites and enhanced ion conduction. Based on these developments, this review systematically elaborates on the component design and ion transport mechanisms of MOFs/polymer nanofiber electrolytes, with a focus on advanced integration strategies beyond physical mixing. This review further discusses combined methods for fabricating MOFs/polymer nanofiber electrolytes and examines the synergistic mechanisms by which MOFs and polymers collectively enhance ionic conductivity and interfacial stability. This review also provides a detailed analysis of current challenges facing MOFs-based composite electrolytes and proposes potential future research directions. By presenting a comprehensive, systematic, and accessible overview of integration strategies and functional mechanisms in diverse MOFs/polymer nanofiber electrolytes, this review aims to inform and inspire the development of high-performance solid-state lithium batteries.

Keywords Electrospinning · Metal–organic frameworks · Nanofiber electrolytes · Interface engineering · Ion transport · Solid-state lithium batteries

1 Introduction

In recent years, the depletion of fossil fuels and increasingly environmental challenges have accelerated the development of eco-friendly, economically viable, and sustainable energy storage systems [1]. Among these, lithium-ion batteries have attracted the most attention owing to their high energy and power densities, making them suitable for portable electronics, electric vehicles, and stationary power stations [2–4]. However, commercial lithium-ion batteries are approaching their maximum theoretical energy density, fundamentally limited by the inherent capacity of graphite anodes of 372 mAh g^{-1}, which severely impedes further progress. Recognized as one of the most promising candidates for next-generation energy storage, lithium metal batteries (LMBs) offer an ultrahigh theoretical specific capacity of 3860 mAh g^{-1} and the lowest electrochemical potential (− 3.04 V vs. the standard hydrogen electrode) among all anode materials [5–7]. Nevertheless,

Xuemeng Gan, Liangjie Gu, and Panpan Dong have contributed equally to this work.

✉ Panpan Dong
panpan.dong@swjtu.edu.cn

✉ Weiqing Yang
wqyang@swjtu.edu.cn

[1] Key Laboratory of Advanced Technologies of Materials (Ministry of Education), School of Materials Science and Engineering, Research Institute of Frontier Science, Southwest Jiaotong University, Chengdu 610031, China

[2] School of Metallurgy and Environment, Engineering Research Center of the Ministry of Education for Advanced Battery Materials, Central South University, Changsha 410083, China

[3] School of Mechanical and Materials Engineering, Washington State University, Pullman, WA 99164, USA

Published online: 18 March 2026

serious safety concerns hinder the widespread adoption of conventional liquid-electrolyte-based LMBs. A key factor is the electrolyte composition typically incorporating flammable organic solvents and thermally fragile lithium salts, which collectively raise risks of thermal runaway and fire [8, 9]. In contrast to conventional LMBs, solid-state lithium metal batteries (SSLMBs) exhibit superior performance characteristics, including: (1) enhanced safety due to the elimination of flammable organic electrolytes, (2) higher theoretical energy density enabled by the compatibility with high-voltage cathodes and lithium metal anodes, and (3) an extended operational temperature range owing to the improved thermal stability of solid-state electrolytes [10, 11]. Because of these advantages, SSLMBs have been extensively studied by researchers [12].

Solid-state electrolytes (SSEs) form the foundation of safety, high-energy-density solid-state lithium metal batteries [13, 14]. By replacing volatile and flammable liquid electrolytes and inhibiting lithium dendrite growth, SSEs substantially improve the intrinsic safety of the battery system [15]. In general, SSEs primarily include polymers, oxides, sulfides, halides, and MOFs [16–19]. Among them, MOFs show great potential as solid electrolytes due to their tunable pore structures, offering an ideal platform for efficient ion transport SSEs [20, 21]. However, their inherent rigidity and crystalline nature lead to poor film-forming ability and inadequate interfacial contact with electrodes, limiting their standalone application [22–24]. Therefore, combining MOFs with other functional materials is an innovative way at present; the advantages of the two materials are complemented. There is a mainstream trend to introduce appropriate polymer into MOFs through a reasonable molding technology [25]. On the one hand, it is precisely because MOFs have unique dimensional/size selectivity of the porous structure that MOFs as fillers can restrict movement of negative ions and promote lithium-ion migration. Additionally, the abundant metal active sites within MOFs are capable of interacting with lithium salts and polymers, thereby facilitating the dissociation of lithium salts, anchoring anions, attenuating the affinity between lithium ions and polymers, and particularly contributing to the realization of molecular design and hybridization of MOFs with polymers [26–30].

Electrospinning technology [31, 32], distinct from conventional physical mixture [33, 34] and other fabrication methods [35–37], enables nanoscale hybridization of MOFs and polymers through either *in situ* incorporation or post-electrospinning functionalization. The composite nanofiber membranes with uniform MOFs dispersion, massloading, and optimized structural integrity via electrospinning. These structural advantages are key for high-performance SSEs, facilitating rapid Li^+ transport and stabilizing the electrolyte interface while suppressing electrolyte decomposition [38, 39]. Hence, electrospinning shows great potential for the development of high-performance solid composite electrolytes (SCEs) [40, 41]. The development of electrospinning for MOFs/polymer composites is summarized in Fig. 1. By *in situ* microwave irradiation, Hatton et al. [42] first reported vanadium(III) benzene-1,4-dicarboxylate MOFs (MIL-47) growing on polyacrylonitrile (PAN), opening up a new path for the application of MOFs/polymer hybrid materials. Inspired by this work, more and more scientists introduce the MOFs/polymer into electrospun nanofibers and apply to various fields [43–47]. The MOFs/polymer electrospun nanofiber membranes exhibit multiple advantages: (1) By confining MOFs in electrospun nanofibers, this strategy addresses the intrinsic issues of particle aggregation and limited recyclability in pristine MOFs materials. (2) By integrating MOFs' tunable crystallinity with polymer nanofibers' structural benefits (e.g., flexibility, morphological control, and lightweight), MOFs/polymer composites achieve a synergistic "rigid-yet-flexible" characteristic [48–55]. (3) Electrospun polymer nanofibers serve as an excellent matrix for supporting MOFs materials, owing to their high mechanical strength and abundant porous structures, which facilitate the fabrication of self-standing MOFs composite films [56–58]. Electrospinning MOFs/polymer composites are overcoming intrinsic issues like aggregation and poor recyclability. By integrating the tunable crystallinity of MOFs with the structural benefits of polymer nanofibers, electrospinning enables synergistic production of flexibility yet mechanically robust SCEs. Additionally, the nanofibers provide robust mechanical support and abundant porosity, which facilitate the film-forming ability of MOFs, highlighting their significant application potential. Therefore, MOFs/polymer nanofiber membranes serve as versatile functional materials that significantly broaden the application scope of MOFs, particularly in environmental and electrochemical energy storage systems.

Herein, this review provides a comprehensive overview of recent advances in the preparation of MOFs-based composite solid electrolytes using the electrospinning technique. We discuss two distinct strategies for integrating MOFs with polymers, and offers insights into how electrospun MOF-based electrolytes can effectively address critical challenges such as dendrite suppression and interfacial instability. Furthermore, we propose potential directions for future research, including the structural modification of MOFs, the exploration of novel polymer matrices, and the optimization of interfacial compatibility between MOFs and polymers, all aimed at enhancing overall performance and practical applicability of SSLMBs.

2 Electrospinning Techniques for MOFs-Based Composite Electrolytes

2.1 Principles of Electrospinning

During electrospinning process, precursor solution at the needle tip becomes charged under an elevated voltage and

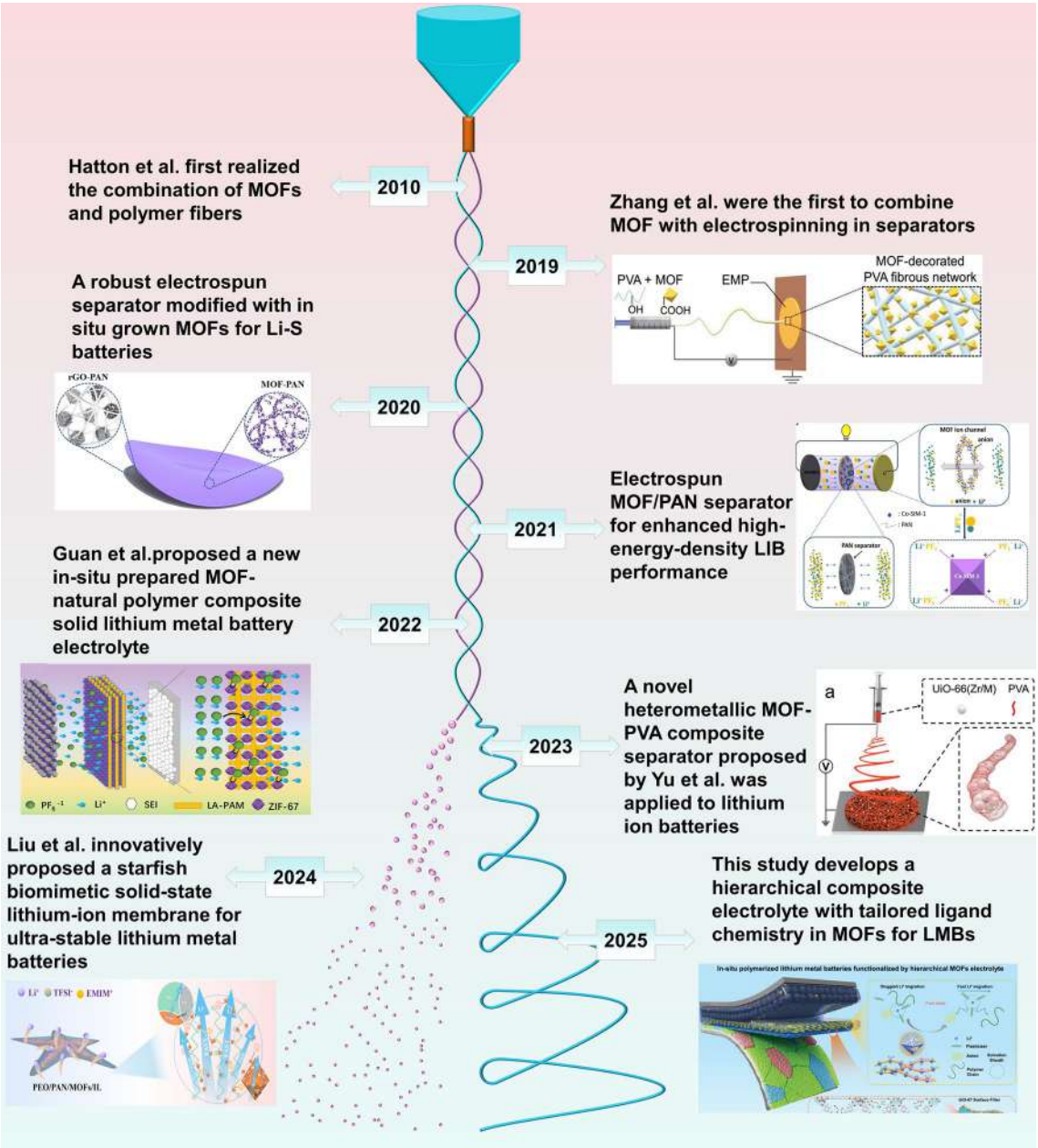

Fig. 1 The timeline shows the key events of combining MOFs and polymer through electrospinning technology in high-performance lithium-based batteries. The combination of MOFs and polymer fiber was realized for the first time in 2010. Reproduced with permission [42]. Copyright 2010, American Chemical Society. The schematic diagram of MOFs-PVA (polyvinyl alcohol) composite membrane prepared by electrospinning for the first time. Reproduced with permission [59]. Copyright 2019, Wiley–VCH. Schematic of the multifunctional electrospun MOFs-PAN/rGO-PAN (rGO refers to reduced graphene oxide) separator and PP (polypropylene) separator for lithium–sulfur batteries. Reproduced with permission [60]. Copyright 2020, Elsevier. Ionic conduction process and anion adsorption process of MOFs in Co-SIM-1/PAN separator (Co-SIM-1 refers to an MOF with unique "wine shelf" structure based on cobalt and trimesic acid). Reproduced with permission. Reproduced with permission [61]. Copyright 2021, Elsevier. The schematic diagram of ion transport mechanism of ZIF-67-LA-PAM (ZIF-67 refers to zeolitic imidazolate framework-67; LA-PAM is composed of lithium alginate and polyacrylamides) separator. Reproduced with permission [62]. Copyright 2022, Wiley–VCH. Schematic of fabrication of composite separators using the electrospinning technique. Reproduced with permission [63]. Copyright 2023, Wiley–VCH. Schematic diagram illustrating the mechanism of rapid Li^+ migration in FAEI (composed of iron 1,4-benzenedicarboxylic acid MOF, PAN, PEO (polyethylene oxide) and Li-IL (lithium-salt-loaded ionic liquid)). Reproduced with permission [64]. Copyright 2024, Wiley–VCH. The composition and functional mechanism of hierarchical MOFs electrolyte. Reproduced with permission [65]. Copyright 2025, Wiley–VCH

thus generates electrostatic forces [66]. Once these forces surpass the liquid's surface tension, the droplet deforms into a conical structure known as a Taylor cone [67]. With further increase in voltage, the intensified electric field exceeds the stabilizing role of surface tension, causing a linear jet to be ejected from the cone apex. After ejection, rapid solvent evaporation and charge dissipation destabilize the jet, leading to radial thinning and the emergence of multiple subsidiary jets. Driven by electrostatic repulsion, the jet undergoes bending instability as it travels toward the collector. Throughout this process, ongoing solvent evaporation promotes solidification, while continuous electrostatic stretching facilitates the formation of ultrafine, continuous nanofibers that deposit on the collector [68, 69].

2.2 Critical Processing and Material Parameters for Electrospun Nanofibers

The morphology, structure, and functionality of electrospun nanofibers are primarily determined by three key factors: (a) the properties of precursor solution, such as viscosity, conductivity, and polymer molecular weight; (b) the processing parameters, including applied voltage, solution feed rate, needle-to-collector distance, and ambient conditions; and (c) the applied post-treatments, like thermal treatment, mechanical pressing, and surface functionalization [70].

2.2.1 Precursor Solution

The morphology of electrospun fibers is greatly determined by the rheological and electrical properties of precursor solution, such as polymer concentration, molecular weight, viscosity, electrical conductivity, and surface tension. Specifically, the critical threshold for fiber fragmentation induced by low solution viscosity is intrinsically governed by polymer concentration. For example, solutions with a viscosity below 8 wt.% (0.5 Pa·s) lack sufficient cohesion to overcome surface tension in PAN system, resulting in "bead-on-string" morphologies instead of continuous fibers [71]. Under such low-viscosity conditions, the jet exhibits significant diameter fluctuations, leading to premature fracture. In contrast, when the viscosity exceeds 2 Pa·s, excessive viscous resistance prevents the formation of a stable Taylor cone, as the electric field can no longer overcome the critical shear stress for jet initiation. Therefore, a viscosity range of 0.5–2 Pa·s is optimal for continuous electrospinning. Within this range, a balance is achieved between electrohydrodynamic stretching and viscoelastic resistance, which facilitates stable jet ejection and suppresses the Plateau-Rayleigh instability. Additionally, electrical conductivity is critical for forming a stable electrified jet. Adding conductive salts, ionic solutions, or metal ions can enhance charge density of polymer precursor solution, which promotes more effective jet elongation and thinning under the electric field to yield ultrafine fibers. Surface tension is another key parameter and must be maintained within a moderate range (approximately 20–50 mN m^{-1}). Insufficient surface tension causes the jet to break into droplets, compromising fiber continuity, whereas excessive tension resists adequate stretching and thinning. Therefore, the composition and properties of the precursor solution directly govern the fiber formation process and ultimately determine the structure and properties of nanofibers [72].

The properties of electrospun fibers can be tailored by selecting specific polymer systems, such as PAN or poly(vinylidene fluoride-co-hexafluoropropylene) (PVDF-HFP). The precursor solution plays a decisive role in this process, as its composition and physicochemical properties are pivotal for controlling both the spinning dynamics and the final fiber structure and performance [71, 73]. Typically, the precursor solution consists of three key components: a polymer matrix, a solvent medium, and functional additives [74]. First, polymers, such as polyvinylpyrrolidone (PVP), polyvinyl alcohol (PVA), and PAN, form the continuous phase of the solution, while the type, molecular weight, and molecular weight distribution of the precursor solution directly govern the solution's rheological properties (e.g., viscosity), fiber-forming capability, and the final fiber's mechanical and functional properties. Solvents (e.g., water, dimethylformamide (DMF), acetonitrile) act as the medium, whose properties govern viscosity, surface tension, and evaporation kinetics to control jet formation. Furthermore, additives, such as plasticizers, salts, or functional molecules, are incorporated to modify processability or introduce advanced functionalities [75, 76].

2.2.2 Process Parameters

Electrospinning process parameters, such as applied voltage (V), flow rate (Q), collector rotational speed (rpm), and working distance (H), are critical in shaping fiber morphology. The morphology of electrospinning nanofibers is critically dependent on precise control of key process parameters [77]. Applied voltage (V): Insufficient voltage fails to overcome solution surface tension, resulting in no fiber formation, unstable jetting, irregular fiber diameters, and fiber adhesion. An optimal voltage range (e.g., 10–15 kV) promotes stable jetting, concentrated diameter distribution, and uniform fibers [78, 79]. Excessively high voltage generates overpowering electrostatic forces, prolonging droplet stretching. This can lead to discontinuous fiber formation and bead defects, as the ejection rate cannot match the rapid stretching. Flow rate (Q): An excessively low flow rate reduces solute mass ejected per unit time, preventing complete encapsulation of the core solution. Subsequent calcination yields beaded or bead-rod structures

instead of continuous hollow nanofibers. An optimal core flow rate (e.g., 0.15 mm min^{-1}) facilitates stable Taylor cone formation, smooth fiber surfaces, uniform diameters, and well-defined hollow carbon nanofibers. An excessively high flow rate impedes complete core encapsulation by the shell solution, causing core solution ejection. This results in bubble formation on fiber surfaces after calcination and the deposition of blocky structures, detrimentally affecting process continuity and fiber morphology. Collector rotation speed (rpm): Inadequate rotation speed reduces collection efficiency, causing fiber pile-up, mutual adhesion, and compromised morphology. Moderate rotation ensures uniform fiber deposition and alignment, yielding superior fiber morphology [80]. Excessive rotation subjects fibers to damaging centrifugal forces, causing breakage, deformation, and compromised diameter/morphology uniformity.

As shown in Fig. 2a, the rotation speed of electrospinning was increased from 800 to 4500 r/min, resulting in highly aligned PAN nanofibers (Fig. 2b–c), which were further modified with $Li_{6.4}La_3Zr_{1.4}Ta_{0.6}O_{12}$ to realize the concept of an anisotropic solid-state polymer electrolyte. This oriented composite structure established a compatible interface with the lithium anode by homogenizing lithium-ion flux, forming a physical barrier to suppress lithium dendrite growth, and delaying side reactions between the electrolyte and lithium. Working distance (H): An insufficient distance allows insufficient solvent evaporation before fiber deposition, causing severe fiber fusion and flattening. An optimal distance (e.g., 15–20 cm) allows complete solvent evaporation and facilitates uniform, continuous fiber formation with concentrated distribution under electrostatic stretching. An excessively large distance increases jet bending instability, causing fiber overlap, increased fiber diameters, and ultimately, discontinuous fiber formation due to insufficient electrostatic force for jet ejection and stretching. Therefore, meticulous optimization of voltage, flow rate, collector speed, and working distance within their respective optimal windows is paramount for achieving targeted fiber morphology [81, 82].

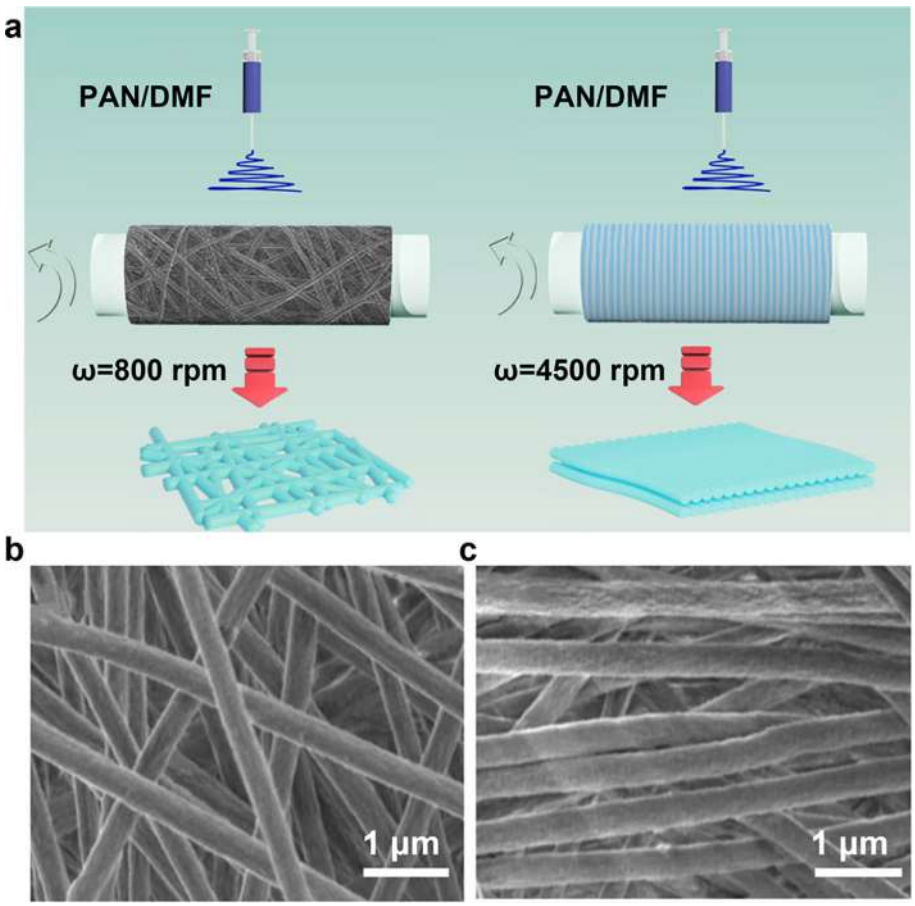

Fig. 2 **a** Schematic diagram of the electrospinning procedure with variable collector rotational speed (800–4500 rpm). **b–c** Scanning electron microscope (SEM) images of surface morphology: scale bars, 1 μm. Reproduced with permission [80]. Copyright 2025, Springer Nature

2.3 Electrospinning for High-Performance MOFs/Polymer Nanofiber Electrolytes

Electrospun nanofibers typically exhibit high aspect ratios and random deposition, forming flexible, bendable, and independent grids characterized by nanoscale vacancies between individual fibers [83, 84]. Due to the operational versatility of electrospinning technology, nanoparticles can be seamlessly integrated into electrospun nanofibers either during the electrospinning process itself or through post-processing of as-spun nanofibers. Additionally, various strategies, such as the sol–gel method, gas–solid reactions, *in situ* photoreduction, and emulsion electrospinning, can be combined with electrospinning to fabricate one-dimensional functional composites, thereby imparting additional functionality and enhanced performance across a wide range of applications [85–87].

Polymer nanofibers can become the most ideal framework for MOFs materials because of their large specific surface area, high porosity, high mechanical strength, and good permeability [88]. The electrospun nanofiber framework can effectively improve lithium-ion transport in electrolyte, increased the Li-ion migration number and lithium-ion conductivity. In addition, the introduction of MOFs particles reduced the decomposition of the electrolyte and promoted the electrode reaction kinetics [89].

For SSEs, high shear modulus was expected, as Newman and Monroe predicted the dendrite growth can be suppressed when the shear modulus of SSEs is large enough [90]. Another requirement for SSEs is the ability to accommodate the stress from battery assembly and the cycling process. During battery cycling, dendrite growth and crack formation may happen [91]. When appropriate polymers and necessary molding technologies are introduced into MOFs, polymers can not only serve as adhesives, and enhance the mechanical properties of composite materials, but also ensure the chemical stability of materials. The as-obtained composites retain the characteristics of uniform porosity and flexibility, which can effectively expand the application range [92].

Actually, for most SSEs, an interphase layer is already formed before battery operation. However, the subsequent reaction behavior of Li/SSEs interphases during charge/discharge should also be considered, as the dynamic variation of Li/SSEs interphase during charge/discharge may also play a role in electrochemical performance of batteries, like solid electrolyte interphase evolution in conventional LMBs. It should be noted that the oxidation of SSEs originates from the instability of their anions, which makes it difficult to suppress the reduction by regulating composition.

3 Research Advances of Electrospun MOFs/Polymer Composite Electrolytes

Polymers, such as PAN, polyvinylidene fluoride (PVDF), and polyethylene oxide (PEO), have been widely reported to prepare high-performance SSEs via electrospinning method [110]. These nanofiber membranes are functionalized with MOFs for synergistic enhancement of electrochemical-mechanical properties. With the aim of constructing a three-dimensional (3D) continuous network structure featuring ion-mechanical synergistic reinforcement, this strategy enables the programmable design and controllable fabrication of high-performance SCEs [112]. This strategy thereby enables the rational design and controllable fabrication of high-performance SCEs. In recent years, a large number of scientific researchers have actively invested in the research of SCEs and have done a lot of work [113].

The integration of MOFs with diverse polymeric systems is predominantly through two distinct methodologies, as illustrated in Fig. 3 and summarized in Table 1. One is direct dispersion of MOFs into the polymer spinning solution, followed by electrospinning to embed them within nanofibers, named MOFs incorporated in polymer nanofiber. The alternative and currently predominant approach begins with fabricating polymeric precursor nanofibers via electrospinning, and then proceeds to the in situ synthesis of MOFs directly on the nanofiber membrane, named in situ growth of MOFs on polymer. The detailed electrochemical properties of reported MOFs/polymer nanofiber electrolytes are compared in Tables S1 and S2 in Supporting Information. Based on the comprehensive comparison, UiO-66 has become the most extensively studied MOFs in recent years. The enhancement mechanism of UiO-66 primarily stems from its stable zirconium-oxo clusters, functionalizable organic linkers, and tunable mesoporous structure, which synergistically improve the ionic conductivity, lithium-ion transference number, and interfacial stability of composite electrolytes. Compared to other common MOFs, UiO-66 not only exhibits excellent thermal and chemical stability but also contains $Zr_6O_4(OH)_4$ clusters that provide abundant Lewis acid sites, effectively promoting lithium salt dissociation and suppressing anion migration. Furthermore, linker modifications, such as the introduction of $–SO_3$, H, $–NH_2$, or other functional groups, can further regulate the interaction between UiO-66 and the polymer matrix, thereby optimizing ion transport pathways. These structural advantages collectively enable UiO-66 to demonstrate relatively superior overall performance among various MOF-based fillers, making it particularly suitable for high-voltage and long-cycle-stable solid-state electrolyte systems.

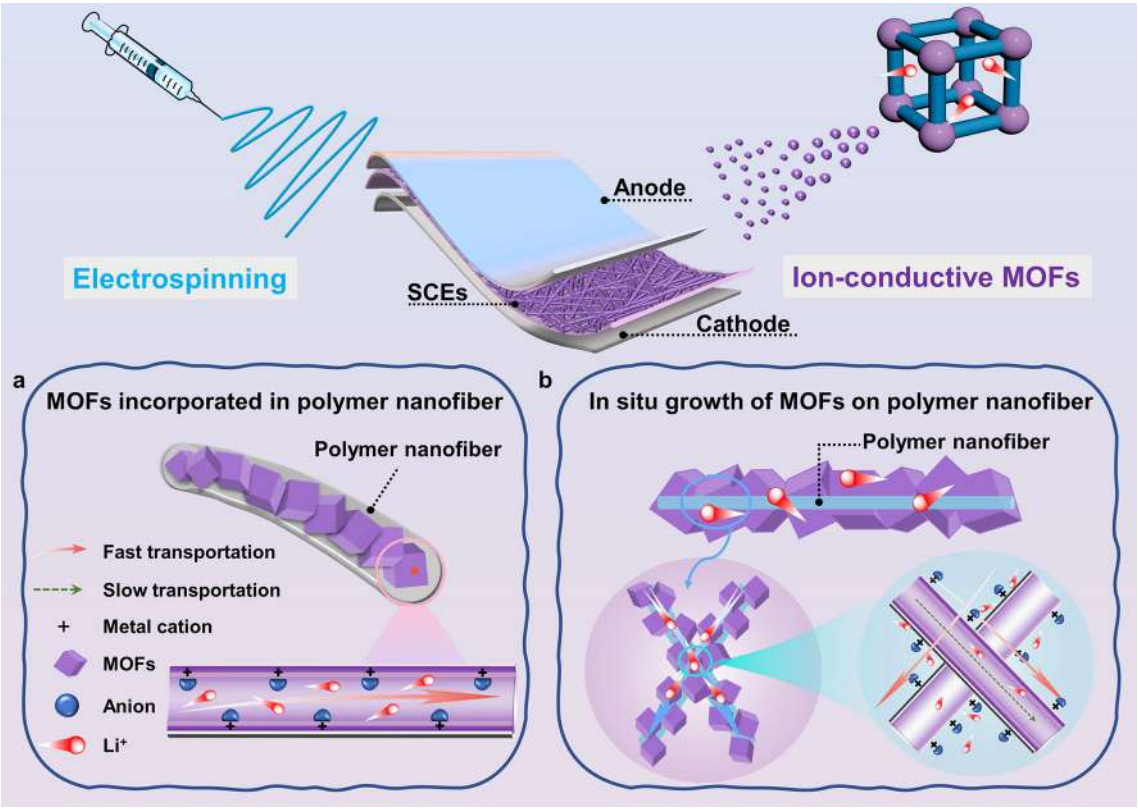

Fig. 3 The integration of MOFs with various polymer systems primarily employs two distinct strategies: **a** MOFs incorporated in polymer nanofiber, where ion transport predominantly occurs within the fiber interior. **b** In situ growth of MOFs on polymer nanofiber, where ion transport mainly takes place along the fiber exterior. SCEs refers to solid composite electrolytes

3.1 MOFs Incorporated in Polymer Nanofiber

3.1.1 MOFs Incorporated in PAN Nanofiber

PAN exhibits a wide electrochemical window, robust mechanical flexibility, and high thermal stability in MOFs/polymer nanofiber electrolytes, showing great potential for next-generation SSLMBs owing to its high compatibility with high-voltage cathodes [114]. Additionally, the effective incorporation of MOFs into the PAN matrix substantially augments electrochemical performance, establishing it as a highly promising candidate for advanced SCEs. The most prevalent method of MOFs integrate with PAN is dispersing MOFs into electrospinning precursor solutions directly. This process enables a homogeneous distribution of MOFs within the PAN matrix, thereby forming a MOFs/PAN composite nanofiber network.

Based on the above mentioned, a novel bio-inspired strategy was applied to MOFs/PAN nanofibers to further improve their interface compatibility. For instance, Ma et al. [64] first developed a bio-inspired 3D SCEs modeled the starfish structure. As illustrated in Fig. 4a, the bio-inspired "starfish-like" SCEs are composed of PAN, MOFs, and ionic liquids (ILs) embedded within a PEO matrix, fabricated via combined electrospinning and casting approach. The process began with synthesized dodecahedral Fe-BDC, which exhibited uniform morphology and good homogeneity (Fig. 4b). These Fe-BDC were subsequently blended with PAN and electrospinning into a continuous 3D membrane, establishing efficient pathways for Li^+ transport. Figure 4c–d confirms the uniform distribution of Fe-BDC along PAN nanofibers without noticeable aggregation. This structural integrating the rigidity of MOFs, the flexibility of PEO, and the interfacial compatibility of ILs. As a result, the SCEs enables a uniform Li^+ flux (Fig. 4e), achieves a high Li^+ transference number ($t_{Li}{}^+ = 0.69$), and delivers an ionic conductivity of 4.37×10^{-4} S cm^{-1} at room temperature. Remarkably, Li/Li symmetric cells equipped with this SCEs demonstrated stable cycling for over 1300 h, reflecting exceptional interfacial compatibility with lithium metal and effective dendrite suppression. In full cells' configurations ($LiFePO_4$ (LFP)/SCEs/Li), the material retained approximately 90.1% of its initial capacity after 2100 cycles at 1 C, while delivering a specific capacity of 146.1 mAh g^{-1} at 60 °C. The bio-inspired "starfish-like" SCEs represents a notable innovation in both material architecture and electrochemical performance, offering

Table 1 Electrospinning parameters and mechanics performances of reported MOFs/polymer electrolytes

Materials			Electrospinning parameter			Mechanical property		Refs.
Polymer	MOFs	Viscosity (wt.%)	Feeding rate (mL h^{-1})	Voltage (kV)	Distance (cm)	Thickness (μm)	Young's modulus (MPa)	
[a] PAN	UiO-66	N/A	N/A	10	15	100	819.4	[93]
	MIL-125-NH_2	N/A	N/A	15	15	76	N/A	[94]
	Fe-BDC MOFs	10.5	0.5	10	15	120	29.1	[64]
[b] PAN	ZIF-67	N/A	N/A	12	15	135 ± 5	N/A	[60]
	ZIF-67	N/A	N/A	20	13	90	N/A	[95]
	UiO-66-SO_3Li	10	1.0	20	15	N/A	2.225	[96]
	MOFs808	10	0.01 mm s^{-1}	15	N/A	90	20.84	[97]
	UiO-66-NH_2	7.4	1.2	20	N/A	90	5.5	[98]
	HKUST-1	7.1	0.12 mm min^{-1}	11.2	18	58	2.7	[99]
	ZIF-8	17	0.6	18	15	120	N/A	[100]
[b] PAN	MOFs/COFs	N/A	1.0	15	15	200	21.19	[101]
[b] PAN/PVA	ZIF-8	10	0.6	18	18	25	3.05 GPa	[102]
[b] PAN/PVP	HKUST-1	10	0.6	20	16	43	16.67	[103]
[a] PVDF-HFP	ZIF-8	N/A	N/A	N/A	N/A	56.92	N/A	[104]
	ZIF-8	4.8	0.6	20	15	45	4.93	[105]
	HKUST-1	11.1	0.6	15	13	40	6.7	[106]
	ZIF-8	11.1	0.04	14	15	52	13.7	[107]
	UiO-66/UiO-67	12.5	3	25	20	95	N/A	[65]
[b] PVDF-HFP	ZIF-67	20	N/A	13	12	86	12	[87]
[a] PMIA	ZIF-67/HKUST-1	25	2	30	17	34	99	[108]
[a] PVA	UiO-66	5	0.6	26	10	60	16.2	[109]
[b] LA-PAM	ZIF-67	5	N/A	20	20	48.9	8.39	[62]
[b] F-PMIA	ZIF-8	N/A	0.1	35	18	120	21.6	[110]
[b] PI	ZIF-8	16	3.6	20	15	47	N/A	[111]

Note: [a] refers to MOFs incorporated in polymer; [b] refers to in situ growth of MOFs on polymer. HKUST-1 = $Cu_3(BTC)_2$; PMIA = Poly(m-phenylene isophthalamide)

extended cycle life and high-temperature operability. Nevertheless, the complexity of its multi-step fabrication process poses a challenge for scalable production, highlighting a key hurdle for practical deployment.

MOFs/PAN electrospun nanofibers can be fabricated through straightforward processes while delivering superior functional properties. For instance, Li et al.[102] engineered a flexible 3D MOFs/PAN SCEs via coaxial electrospinning, in which MOFs were uniformly dispersed on PAN nanofibers. The resulting composite exhibited a high room-temperature ionic conductivity of 1.29×10^{-3} S cm^{-1} and t_{Li}^{+} of 0.79 after in situ thermal polymerization. Moreover, the Zeolitic Imidazolate Framework-8 (ZIF-8) coating on PAN nanofibers significantly improved the reduction tolerance of the membrane against lithium metal, while the high MOFs loading reinforced the Young's modulus of the composite electrolyte up to 1.31 GPa, collectively contributing to effective suppression of lithium dendrites formation and penetration. In summary, although direct electrospinning of PAN/MOF composites represents a versatile and promising strategy for developing high-performance SCEs, strengthening interfacial adhesion, and designing more sophisticated architectures to overcome existing limitations and fully realize their potential in next-generation SSLMBs.

3.1.2 MOFs Incorporated in PVDF Nanofiber

As another widely investigated polymer, PVDF and its copolymers are considered a compelling platform for designing advanced SCEs, owing to their high dielectric constant that promotes salt dissociation, intrinsic mechanical toughness, and broad electrochemical windows [115–117]. In recent years, electrospinning has emerged as a prominent strategy for integrating PVDF with MOFs, establishing such composites as a research frontier in the development of SSLMBs. The incorporation of MOFs into PVDF-based nanofibers significantly enhances ionic conductivity and Li^+ transference numbers, a phenomenon attributable to the

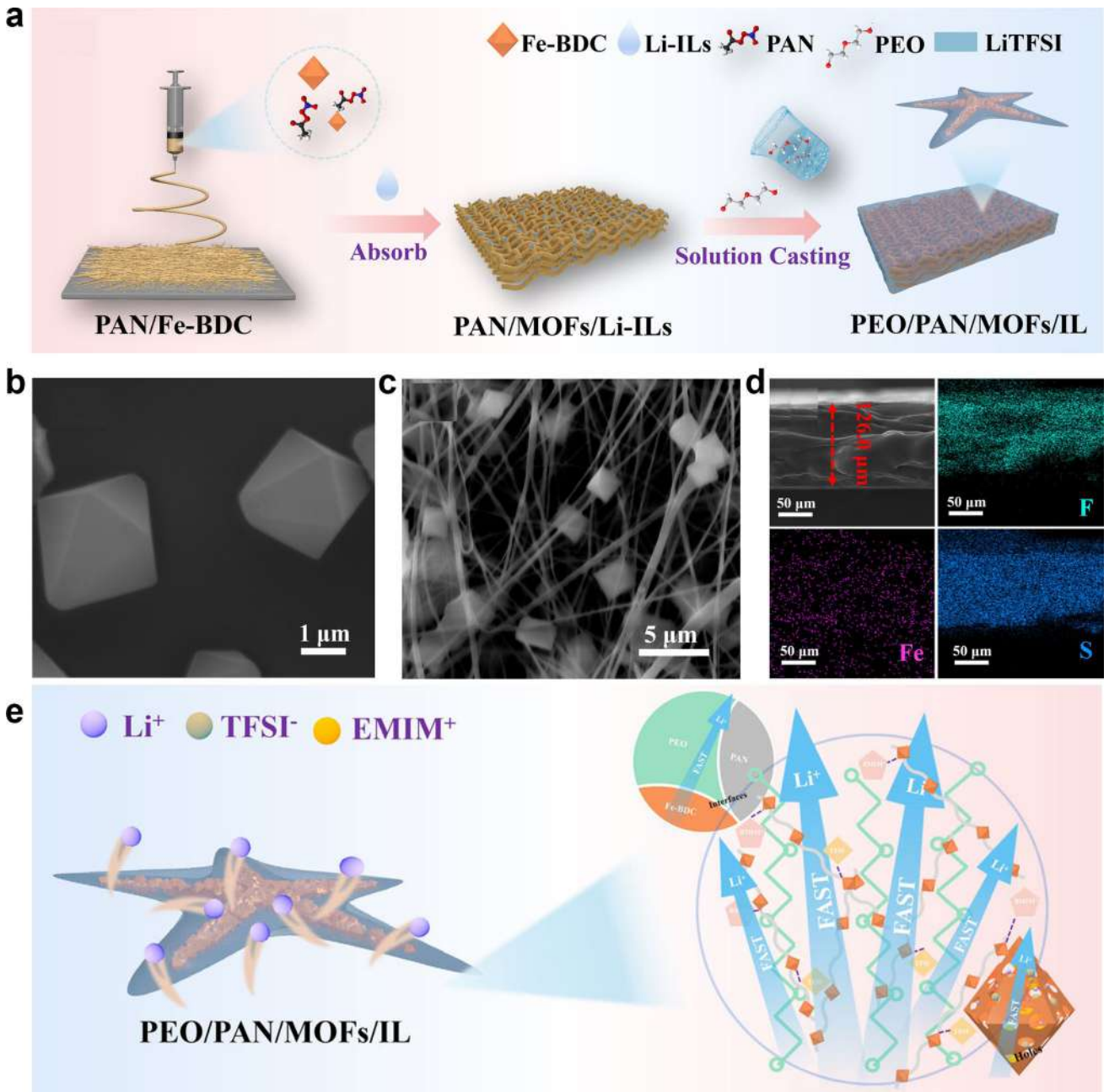

Fig. 4 **a** Bionic conceptual diagram of the starfish-inspired solid-state electrolyte and the multifunctional synergistic mechanisms of the PEO/PAN/MOFs/IL (MOFs refers to iron 1,4-benzenedicarboxylic acid MOF; IL = ionic liquid) film, LiTFSI = lithium bis(trifluoromethanesulfonyl)imide. The SEM images of **b** Fe-BDC MOF particles and **c** MOFs incorporated in PAN composite. **d** Cross-sectional SEM with Energy-Dispersive Spectroscopy (EDS) mapping of solid-state electrolyte. **e** Schematic diagram illustrating the mechanism of rapid Li^+ migration in solid-state electrolyte. Reproduced with permission [64]. Copyright 2024, Wiley–VCH

intrinsic porosity and Lewis acid sites of MOFs, which facilitate anion immobilization and promote ion-pair dissociation [105, 118]. Furthermore, the synergistic interaction between MOFs and PVDF-HFP effectively suppresses polymer crystallization, thereby facilitating Li^+ migration. Concurrently, the in situ formation of a LiF-rich interphase resulting from PVDF-HFP decomposition serves as a protective barrier against interfacial side reactions. These integrated mechanisms collectively contribute to the formation of a highly stable electrode–electrolyte interface [119].

Among various MOFs, ZIF-8 stands out as one of the most extensively studied materials. On one hand, ZIF-8 serves as a multifunctional nanofiller that significantly enhances the mechanical strength and thermal stability of

PVDF-HFP nanofibers, owing to its rigid porous architecture and strong interfacial adhesion with the polymer matrix. On the other hand, its high specific surface area and uniform microporosity further impart the composite fibers with improved adsorption capacity, molecular sieving capability, and even catalytic activity [120]. A representative example was reported by Fan et al. [104], who constructed a 3D MOFs/PVDF-HFP fibers network. The resulting network was subsequently embedded into a PEO/LiTFSI/ILs (1-ethyl-3-methylimidazolium bis(trifluoromethanesulfonyl) imide) to form SCEs denoted as PHML (Fig. 5a–b). The unique structure of the PHML electrolyte, characterized by a continuous 3D MOFs/PVDF-HFP network and further enhanced with ionic liquids, enables superior electrochemical performance. This tailored architecture facilitates rapid Li^+ transport, yielding a high ionic conductivity of 1.36×10^{-4} S cm^{-1} and a $t_{Li}{}^+$ of 0.49 at room temperature (Fig. 5c). Furthermore, the robust mechanical strength of PHML (15.06 MPa) effectively suppresses lithium dendrite growth, as confirmed by the stable polarization voltage and long-term cycling stability in both Li/Li symmetric cells (Fig. 5d) and LFP/Li full cells (Fig. 5e).

While the 3D MOFs/PVDF-HFP architecture has proven effective in conventional LMBs, its design concept also shows promising adaptability to more complex battery chemistries, as exemplified by recent advances in solid-state lithium–oxygen batteries. Li et al. [105] prepared a novel gel electrolyte incorporating ZIF-8 into a PVDF-HFP matrix for solid-state lithium–oxygen batteries (SSLOBs) (Fig. 5f). The resulting gel electrolyte exhibits exceptional performance, with an unprecedented $t_{Li}{}^+$ of 0.88 and a remarkable room-temperature ionic conductivity of 9.13×10^{-4} S cm^{-1} (Fig. 5g–h). Figure 5i–k demonstrates that the ZIF-8/PVDF-HFP electrolytes providing a high discharge capacity of 7189 mAh g^{-1} at 100 mA g^{-1} with low polarization (0.8 V). The system achieves 145 stable cycles, a result of the synergistic combination of MOFs-enhanced ion transport and $Ir(acac)_3$-mediated Li_2O_2 decomposition, while effectively suppressing mediator shuttling.

Compared with the above single-layer composite solid electrolyte, it is necessary to design a multi-layer composite solid electrolyte that can provide enhanced interface compatibility, mechanical integrity, and electrochemical stability. For example, Chai et al. [106] prepared a flexible asymmetric composite polymer electrolyte (denoted as PPH-SSE) containing MOFs filler, 3D PAN/PVDF-HFP bilayer nanofibers was prepared via electrospinning and *in situ* polymerization (Fig. 6a). The high-performance asymmetric SCEs with a gradient interface design effectively address the compatibility issue between the high-voltage cathode and the lithium metal anode. As illustrated in Fig. 6b, the Li/$LiNi_{0.8}Co_{0.1}Mn_{0.1}O_2$ (NCM811) coin cell equipped with PPH-SSE delivers the highest discharge specific capacities at various current rates (ranging from 0.1 to 5 C) and exhibits excellent capacity recovery when the rate is reverted to 0.1 C, outperforming the cells with PH-SSE (PAN@HKUST-1 nanofiber membranes) and C-SSE (Commercial Celgard 2500 separator). In comparison, Tan et al. [107] leveraged electrospinning technology to integrate ZIF-8 and PVDF-HFP, constructing a bilayer SCEs (denoted as PPZ). LiTFSI was added to the precursors of the spinning solution. The "pre-lithiation" design can effectively promote the cleavage of C–F bonds and the formation of LiF [121]. This structure combines with ZIF-8@PVDF-HFP as the porous framework and PEO as the Li^+ conductive matrix, aiming to overcome the limitations of PEO-based electrolytes (Fig. 6c). By integrating mechanical and interfacial stability advantages of PVDF-HFP as well as the ion-conduction enhancement benefits of ZIF-8 into PEO matrix, the PPZ exhibits stable high-voltage performance in SSLMBs. As illustrated in Fig. 6d, $LiCoO_2$ (LCO)/PPZ/Li cell delivers a discharge specific capacity of 144.7 mAh g^{-1} at 0.2 C, nearly 1.6 times than that of LCO/PEO/Li (90.7 mAh g^{-1}). In a distinct approach, Lin et al. [65] fabricate SCEs through a multi-step process combining electrospinning, electrospraying, and *in situ* polymerization (Fig. 6e). This structurally tailored design successfully decouples the requirements for high ionic conductivity and interfacial stability. As a result, the HEPE (PVDF@UiO-66d@67 + Poly-1,3-dioxolane (PDOL)) achieves high room-temperature ionic conductivity (0.85×10^{-3} S cm^{-1}), outstanding cycling performance (92.7% capacity retention after 2000 cycles at 2 C in LFP full cells), and high-voltage compatibility (stable operation over 630 cycles when coupled with $LiNi_{0.5}Co_{0.2}Mn_{0.3}O_2$ cathodes) (Fig. 6f). This study offers a novel strategy for addressing ion transport and interfacial stability challenges in SSLMBs through tailored MOFs ligand chemistry. Sun et al. [122] also combined synchronous electrospinning (PAN) and electrostatic spray (UiO-66 suspension) to form PAN/UiO-66 composite membrane. On the basis of the regulating effect of UiO-66, the growth of Li dendrites is significantly restrained and the electrolyte exhibits long-life electrochemical stability with Li anode during the Li plating/stripping.

3.1.3 MOFs Incorporated in Other Polymer Nanofibers

As mentioned earlier, while polymers, such as PAN, PVDF-HFP, and PEO, have been widely utilized as precursors for electrospinning solutions, growing research efforts have explored alternative polymer systems to broaden material versatility and enhance performance. This section systematically summarizes the implications of different binding modes between such emerging polymers and MOFs on the electrochemical behavior of lithium metal

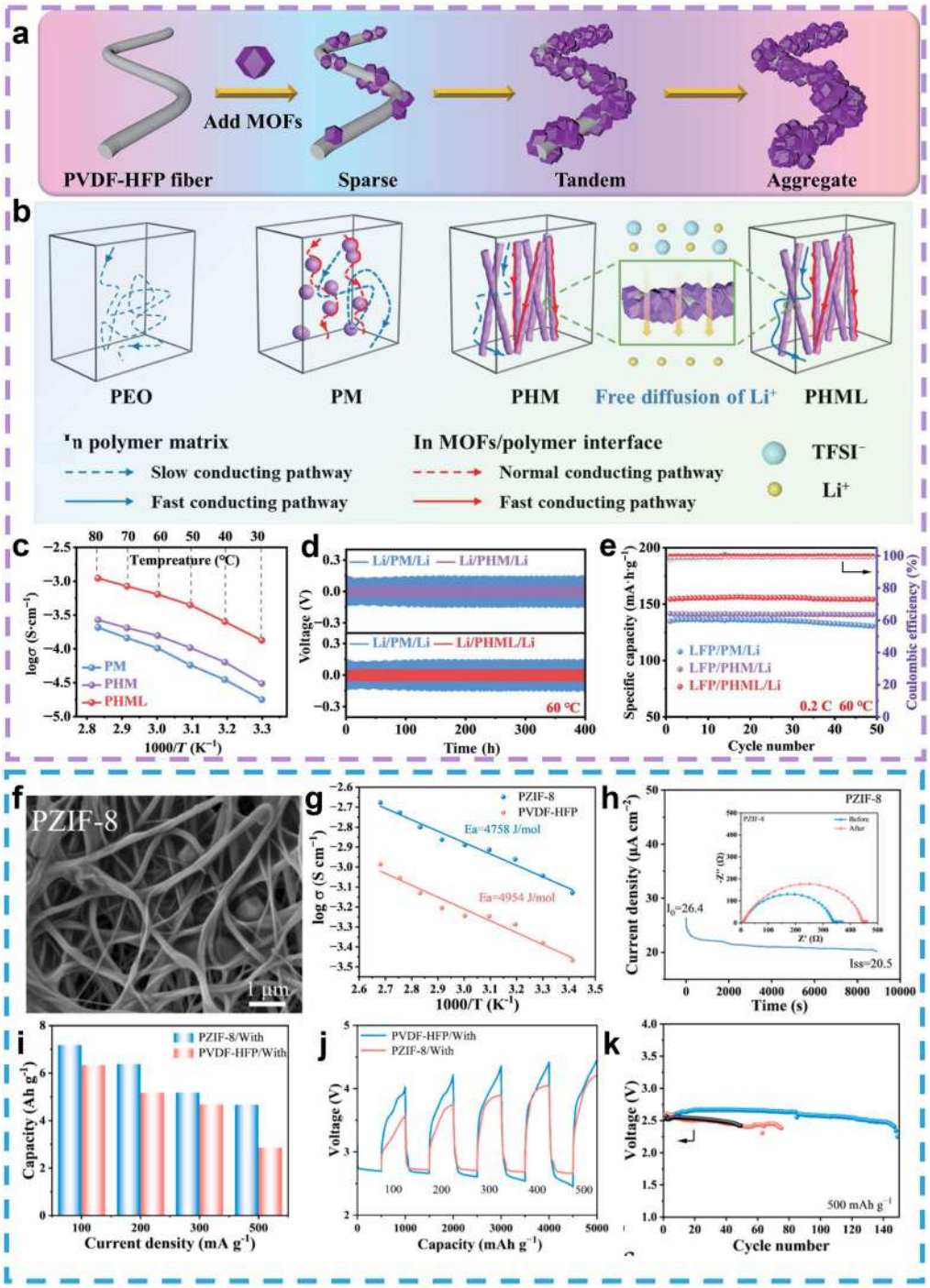

Fig. 5 **a** Schematic diagram of the structural evolution with the change of the ratio between ZIF-8 (Zeolitic Imidazolate Framework-8) and PVDF-HFP. **b** Schematic representation of Li^+ transport in PEO matrix, PM (PEO + ZIF-8), PHM (PEO + PVDF-HFP + ZIF-8), and PHML (PEO + PVDF-HFP + ZIF-8 + IL), respectively. **c** The ionic conductivity of the SCEs was compared. **d** Polarization voltage curves of symmetric Li/Li cells with PHM and PHML electrolytes. **e** Cycling performance of LFP/Li batteries. Reproduced with permission.[104] Copyright 2023, Springer Nature. **f** SEM image of PZIF-8 (PVDF-HFP + ZIF-8). **g** Arrhenius plot of PZIF-8 and PVDF-HFP. **h** The chronoamperometry test for PZIF-8. **i** Rate performance and **j** deep discharge profiles of SSLOBs based on PVDF-HFP/With and PZIF-8/With, set the discharge capacity at 500 mAh g^{-1} and increase the current density from 100 mA g^{-1} to 500 mA g^{-1}. **k** Voltage versus cycle number on the discharge terminal of SSLOBs based on PVDF-HFP/With (black), PZIF-8/With (blue), and PZIF-8/Without (red), with/without refers to whether redox mediators are introduced into the electrolyte. Reproduced with permission.[105] Copyright 2025, Elsevier

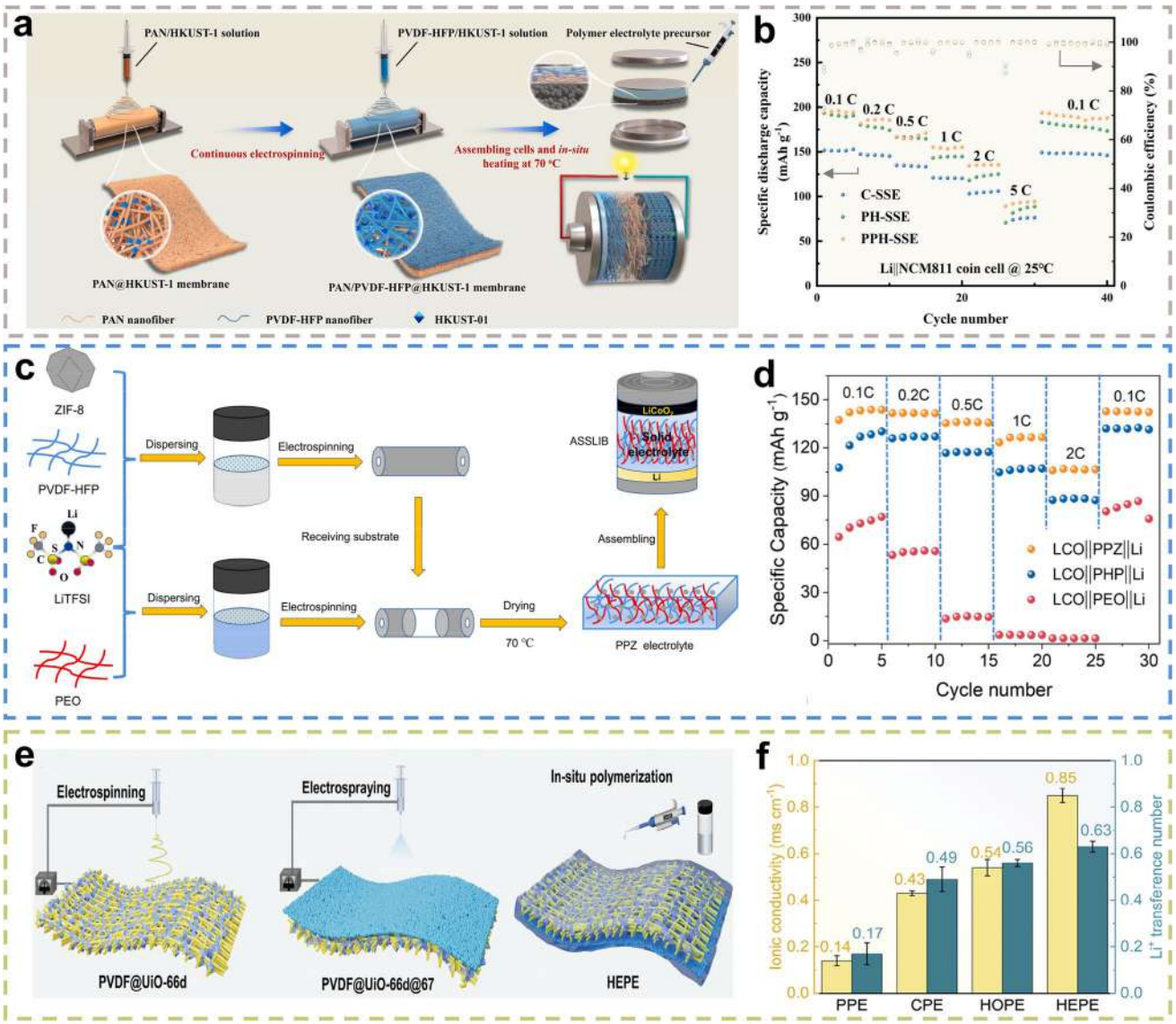

Fig. 6 **a** Schematic of the electrospinning process and *in situ* synthesis route of PPH-SSE (PAN + PVDF-HFP + HKUST-1). **b** Rate capability of Li/NCM811 coin cells with different SSEs (C-SSE (*In situ* polymerization based on commercial Celgard 2500 separator solid-state electrolyte), PH-SSE (*in situ* polymerization based on PAN@HKUST-1 nanofiber membranes solid-state electrolyte), PPH-SSE (*in situ* polymerization based on PAN/PVDF-HFP@HKUST-1 nanofiber membranes solid-state electrolyte), voltage ranged from 2.5 V to 4.3 V, loading was 2.5 mg cm^{-2}. Reproduced with permission [106]. Copyright 2024, Elsevier. **c** Schematic illustration of PPZ (PEO + PVDF-HFP + ZIF-8) electrolyte and all-solid-state battery. **d** Rate performances of LCO/PEO/Li, LCO/PHP (PVDF-HFP + PEO)/Li, and LCO/PPZ/Li batteries. Reproduced with permission [107]. Copyright 2024, Elsevier. **e** Schematic illustration of the preparation procedure of PVDF@UiO-66d nanofiber, PVDF@UiO-66d@67 nanofiber, and hierarchical polymer electrolyte (HEPE = PVDF@UiO-66d@67 + PDOL). **f** Comparison of ionic conductivity and Li^+ transference number of different electrolytes. Reproduced with permission, PPE = PVDF + PDOL, CPE = PVDF@UiO-66d + PDOL, and HOPE = PVDF@UiO-66d@66 + PDOL [65]. Copyright 2025, Wiley–VCH

batteries, with a focus on their underlying Li^+ conduction mechanism.

Poly-m-phenylene isophthalamide (PMIA)-based nanofibers' SCEs demonstrate exceptional thermal stability, self-extinguishing characteristics, electrical insulation properties, and mechanical robustness. Deng et al. [108] introduced modified SCEs by incorporating Co-based ZIF-67 and HKUST-1 into a gel F-doped PMIA nanofiber membranes denoted F-Cu-BTC-PMIA. The SCEs combine high-temperature resistance with effective dendrite suppression, which achieve a high ionic conductivity of 1.96×10^{-3} S cm^{-1} at room temperature. Through the synergistic effects of physical confinement from the gel matrix and chemical adsorption by MOFs, the polysulfide shuttle

effect is significantly suppressed, while a uniform Li^+ flux distribution inhibits lithium dendrite growth (Fig. 7a–b). As a result, lithium–sulfur batteries assembled with these MOFs-modified separators demonstrate excellent cycling stability and rate capability (Fig. 7c), laying a solid foundation for further development of high-performance separators. In another study, Yu et al.[109] fabricated composite separators based on heterometallic MOFs (UiO-66(Zr/Ti) and UiO-66(Zr/Hf)) and PVA via electrospinning (Fig. 7d–e). These heterometallic MOFs, which feature a high density of open bimetal sites and strong anion complexation capability, significantly enhance lithium-ion transport, enabling an ionic conductivity of up to 7.79×10^{-3} S cm^{-1} and a $t_{Li}{}^+$ of up to 0.83 (Fig. 7f). As shown in Fig. 7g–j, lithium-ion batteries equipped with these heterometallic MOFs-based composite separators exhibit significantly improved rate capability (approximately 60% capacity retention at 5 C) and cycling stability (> 70% capacity retention after 1000 cycles at 1 C) compared to traditional polypropylene separators.

In general, the direct blending of MOFs incorporated in polymer remains the predominant method for fabricating SCEs, valued for its simplicity and effectiveness in achieving uniform MOFs dispersion. In this structure, MOFs are uniformly embedded and aligned within the polymer nanofibers, forming a continuous and ordered composite network. This architecture facilitates a directional arrangement of MOF active sites along the nanofibers, enabling fast Li^+ transportation via a fiber-axial mechanism, which not only improves bulk conductivity but also promotes uniform lithium deposition, contributing to superior cycling stability and rate performance in solid-state batteries. Nevertheless, this strategy faces several intrinsic challenges. A major limitation is the difficulty in achieving high MOFs loading without agglomeration, which often compromises membrane flexibility and ionic conductivity. Moreover, the embedding of MOFs within polymer nanofibers fails to fully leverage their structural functionalities, as ion transport between nanofiber bundles can be obstructed. Interfacial incompatibility between MOFs and the polymer matrix may also result in defective zones, ultimately impairing overall electrochemical performance. To address these limitations, advanced strategies such as coaxial electrospinning have been developed to achieve more precise structural control.

3.2 In Situ Growth of MOFs on Polymer Nanofiber

In situ growth of MOFs on polymer nanofibers has emerged as a widely employed strategy, distinguished by its unique structural and functional advantages [123]. This approach typically involves a two-step process beginning with the fabrication of a polymer nanofiber scaffold through electrospinning. Subsequently, MOFs are directly nucleated and grown on the nanofiber surfaces via either solution immersion or vapor-phase deposition, ultimately producing a continuous core–shell composite membrane. This structurally integrated configuration ensures strong interfacial bonding while creating highly ordered ion-conduction pathways along the nanofiber axis. Furthermore, it enables both high MOFs loading and the formation of a density electrolyte framework, collectively contributing to significantly enhanced ionic conductivity and improved mechanical robustness in the resulting SCEs [124].

3.2.1 In Situ Growth of MOFs on PAN Nanofiber

Rather than incorporating pre-synthesized MOFs, the technique of in situ growth of MOFs on PAN utilizes the functional groups on PAN fibers to direct MOFs nucleation and growth. The process begins by incorporating metal salts into the polymer spinning dope prior to electrospinning. The resulting electrospun membrane is then immersed in a solution containing organic ligands and subjected to static incubation, enabling the in situ formation of MOF particles directly on the nanofiber surfaces (Fig. 8a) [103]. Figure 8b1–b3 reveals HKUST-1 particles with an average diameter of approximately 50 nm uniformly distributed and tightly anchored on PAN nanofibers. This structural configuration, achieved through the abundant nitrile and hydroxyl groups on PAN that strongly facilitate HKUST-1 nucleation and growth, results in high MOFs loading and uniform coating (Fig. 8c–d). These structural features endow the composite membrane with superior electrochemical properties, including an elevated $t_{Li}{}^+$ of 0.77, and a high critical current density of 4.5 mA cm^{-2}, significantly outperforming conventionally designed electrolytes (Fig. 8e–f). Notably, Li/Li symmetric cells demonstrate remarkable stability, maintaining operation for over 4000 h at a high current density of 4 mA cm^{-2} (Fig. 8g), highlighting the practical potential of this interface engineering approach.

In a significant development, Xu et al. [97] constructed a 3D PAN network via electrospinning as a supporting scaffold and subsequently grew MOF808 (a 3D continuously interconnected zirconium-based MOF) onto the PAN nanofibers through a hydrothermal method, yielding a 3D interconnected SCEs (Fig. 9a). The resulting architecture features highly ordered MOFs aligned along single nanofiber, which interconnect to form a continuous 3D network (Fig. 9b1–b3). The substantial, strong interaction between the open metal sites on MOF network surface and the anions, thereby releasing more free Li^+ ions. As illustrated in Fig. 9c, the incorporation of this 3D MOFs@PAN network simultaneously enhances the mechanical robustness of the electrolyte and establishes continuous channels for rapid Li^+ conduction. Complementarily, capacity of MOF808 to confine anion migration enables precise regulation of Li^+ flux distribution, leading to an elevated local Li^+

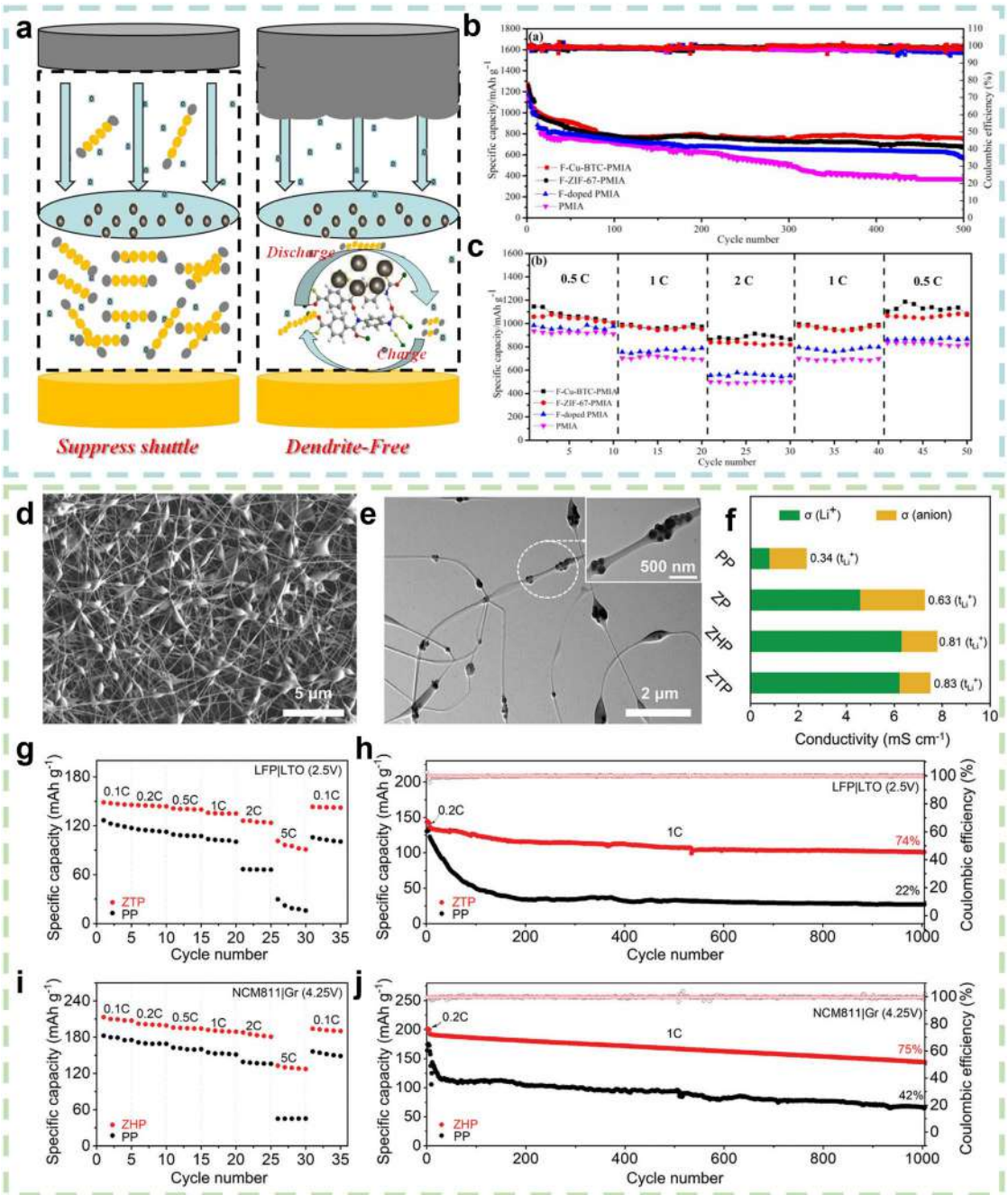

Fig. 7 **a** The schematic illustration of shuttle effect suppression of lithium polysulfides and anode protection in Li–S battery. **b** Battery performance of PMIA, F-doped PMIA, F-ZIF-67-PMIA, and F-Cu-BTC-PMIA membrane at 0.5 C at room temperature; F refers to fluoro-chemical based emulsion. **c** Rate capability of PMIA, F-doped PMIA, F-ZIF-67-PMIA, and F-Cu-BTC-PMIA membrane. Reproduced with permission [108]. Copyright 2020, Elsevier. **d** SEM and **e** TEM images of ZTP (UiO-66(Zr/Ti) + PVA) separator. **f** Partitioned ionic conductivities (Li^+ and anion) and t_{Li}^+ of electrolytes in PP, ZP (UiO-66(Zr) + PVA), ZTP, and ZHP (UiO-66(Zr/Hf) + PVA). **g** Rate performance and **h** cycling performance of LFP/$Li_4Ti_5O_{12}$ (LTO) cells with PP or ZTP (LFP cathode, 11.5 mg cm^{-2}; LTO anode, 12.1 mg cm^{-2}). **i** Rate performance and **j** cycling performance of NCM811/Graphite (Gr) cells with PP or ZHP, NCM811 and Gr electrodes were controlled with areal loading of 4.7 and 8.4 mg cm^{-2}, respectively, which corresponds to an N/P (negative-to-positive capacity ratio) ratio of 1.05. All electrochemical tests were carried out in a 25 °C incubator. Reproduced with permission [109]. Copyright 2023, Wiley–VCH

concentration at the MOFs/polymer interface. This synergistic mechanism facilitates homogeneous lithium deposition and effectively suppresses dendrite formation. Remarkably, the SSLMBs maintains exceptional cycling stability, delivering a discharge capacity of 102 mAh g^{-1} after 1000 cycles at 1 C while retaining 77% of its maximum capacity (133 mAh g^{-1}), as shown in Fig. 9d. This performance underscores the efficacy of the 3D interconnected MOF-based architecture in enabling high-rate capability and long-term cycling stability in SSLMBs.

3.2.2 In Situ Growth of MOFs on PVDF-HFP Nanofiber

Recently, adsorption membranes combining the advantages of adsorption materials and polymer membrane have attracted large interests. For instance, Qi et al. [87] designed a composite solid electrolyte constructed by combining a nanofiber-connected ZIF-67 adsorption membrane with *in situ* polymerized (ethylene glycol) diacrylate (PEGDA)/succinonitrile (SN)/LiTFSI. This designed ZIF-67-incorporated nanofiber adsorption membrane demonstrates both excellent mechanical robustness and the capability to enable uniform lithium plating/stripping while effectively suppressing dendrite growth in Fig. 10a–c. It achieves a high t_{Li}^{+} of 0.63 as depicted in Fig. 10d. In terms of interfacial stability, the Li/PZPS/Li symmetric cell shows stable Li plating/stripping for 920 h at (0.1 mA cm^{-2}), significantly outperforming the Li/PPS/Li cell which fails after 62 h. Furthermore, the LFP/PZPS/Li cell maintains 90% capacity retention after 500 cycles at 0.5 C (Fig. 10e–f).

3.2.3 In Situ Growth of MOFs on Other Polymer Nanofibers

The integration of MOFs with diverse polymer precursors that beyond conventional systems like PAN, PVDF-HFP, and PEO unlocks unprecedented opportunities for designing advanced functional materials with tailored architectures and enhanced performance.

For example, Guan et al. [62] designed a novel MOFs-natural polymer composite electrolyte (ZIF-67-LA-PAM, ZIF-67 refers to zeolitic imidazolate framework-67; LA-PAM is composed of lithium alginate and polyacrylamides). As described in Fig. 11a–b, because of ZIF-67 ordered porous structure provides direct channels for Li^{+} migration, while unsaturated Co sites interact with PF_6^{-} anions via Lewis acid–base interactions, promoting $LiPF_6$ dissociation and increasing the concentration of free Li^{+}. Density Functional Theory calculations confirm that ZIF-67 reduces the binding energy of Li–O bonds in the composite, further facilitating Li^{+} release from the polymer matrix. As a result, the ZIF-67-LA-PAM electrolyte achieves a higher ionic conductivity (3.84×10^{-3} S cm^{-1} at 30 °C) compared to the LA-PAM electrolyte without MOFs (2.84×10^{-3} S cm^{-1}), and t_{Li}^{+} of 0.627 (Fig. 11c). Notably, it was seen from Fig. 11d that Li/ZIF-67-LA-PAM/Li cell maintains the polarization voltage of 0.2 V for more than 1300 h at the current density of 100 mA cm^{-2}.

In a follow-up study, Luo et al. [110] demonstrated a composite electrolyte membrane designed for solid-state lithium metal batteries, fabricated by incorporating Zn-based ZIF-8 nanoparticles into a fluorinated PMIA nanofiber membrane and infiltrating with PEO–LiTFSI. Figure 11e shows the surface and cross-sectional morphology of F-PMIA@ZIF-8. As shown in Fig. 11f, ZIF-8 acts as a multifunctional additive by utilizing its micropores and Lewis acid sites to anchor anions and promote lithium salt dissociation, which enables a high free Li^{+} concentration for superior ionic conduction (2.39×10^{-4} S cm^{-1} at 30 °C). Hereby, F-PMIA@ZIF-8-PEO-LiTFSI exhibits a significantly wider electrochemical stability window compared to the other samples, indicating that the incorporation of dendritic architecture and ZIF-8 effectively enhances the high-voltage stability of the SCEs in Fig. 11g. This LFP/F-PMIA@ZIF-8-PEO-LiTFSI/Li also demonstrates excellent rate capability (Fig. 11h). Interestingly, Lan's team also used ZIF-8 as an organometallic framework. The difference is that this technology closely arranges ZIF-8 nano-units on polyimide (PI) nanofibers through electrospinning and *in situ* self-assembly technology to form one-dimensional ordered MOFs nanofibers and three-dimensional multiscale MOFs networks to facilitate efficient Li^{+} transport (Fig. 11i–j) [111]. The calculated t_{Li}^{+} of 0.88 for PI@ZIF-8 nanofiber separator was much higher than that of PE separator in Fig. 11k. Besides, the LFP/PI@ZIF-8/Li cells showed a distinct advantage in discharge capacity, especially under high-rate conditions. When recovering from a high rate of 5 C to the initial low rate of 0.2 C, they presented good capacity reversibility (Fig. 11l).

In summary, this method of MOFs growth on other polymers is more widely studied. This approach enables the precise construction of hierarchical architectures where MOFs nanoparticles are uniformly anchored onto polymer fiber surfaces through coordination bonding or electrostatic interactions, yielding composites with enhanced ionic conductivity, mechanical strength, and thermal stability. Novel polymers, such as PI, PMIA, PAM, etc., synergize with the pore/site advantages of MOFs through their high thermal/electrochemical stability, and systematically solve the bottlenecks of poor low-temperature lithium conductivity, weak dendrite suppression, and interface instability of traditional matrix (e.g., PAN/PEO/PVDF), providing a feasible strategy for high-energy density solid-state batteries. In the field of solid electrolytes, the composite systems of novel polymer matrices combined with MOFs hold broad prospects for future development. It is feasible to optimize the polymer structure through molecular design, develop specific MOFs to enhance compatibility and ion transport, and conduct

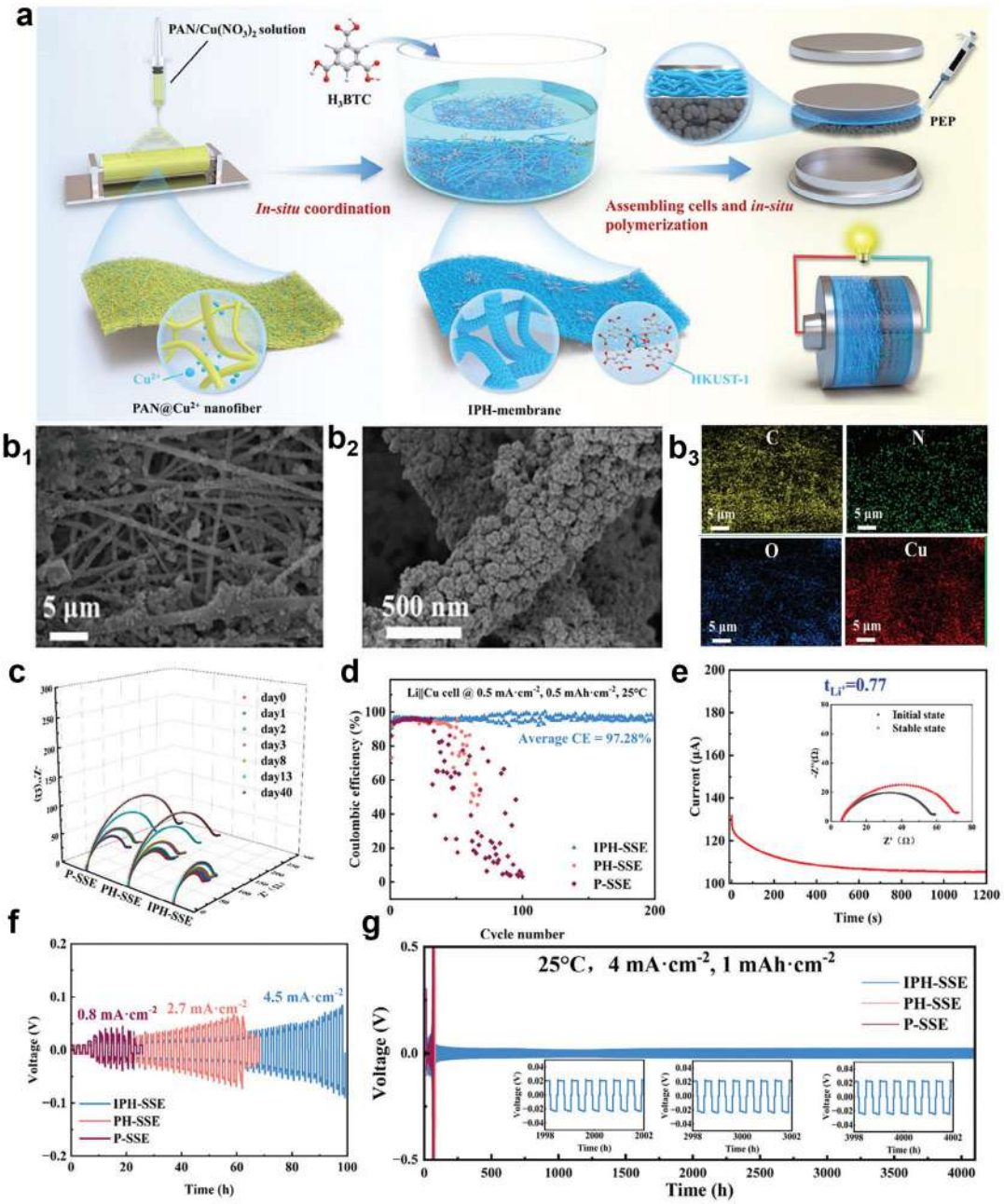

Fig. 8 Preparation of electrolyte membrane and its structural and physicochemical characterizations. **a** Schematic of the electrospinning process and in situ synthesis route of IPH-SSE (in situ coordinated PAN@HKUST-1 SSE) $\mathbf{b_1}$–$\mathbf{b_3}$ SEM images and corresponding EDS mappings of IPH-membrane. **c** Time evolutions of Nyquist plots of Li/Li symmetric cells with different SSEs (P-SSE (Pure PAN-based SSE), PH-SSE (PAN@HKUST-1 Hybrid SSE), IPH-SSE). **d** CEs of Li/Cu cells using different SSEs at 0.5 mA cm^{-2}@0.5 mAh cm^{-2}. **e** Current–time curve of Li/Li symmetric cell with IPH-SSE (inset: Nyquist plots before and after polarization). **f** Galvanostatic cycling curves of Li/Li symmetric cells with different SSEs at different current densities. **g** Galvanostatic cycling curves of Li/Li symmetric cells with different SSEs at 4 mA cm^{-2}@1 mAh cm^{-2} (inset: partial enlarged diagrams at different periods). Reproduced with permission [103]. Copyright 2025, Wiley–VCH

in-depth research on interfacial interactions to establish a structure–activity relationship, thereby addressing the defects of traditional matrices.

The strategy of in situ growth of MOFs on polymer nanofiber demonstrates distinctive advantages in constructing advanced SCEs. Central to this approach is the establishment of robust chemical bonding between MOFs and polymer nanofibers, which significantly enhances interfacial compatibility and effectively circumvents the phase separation commonly observed in conventional

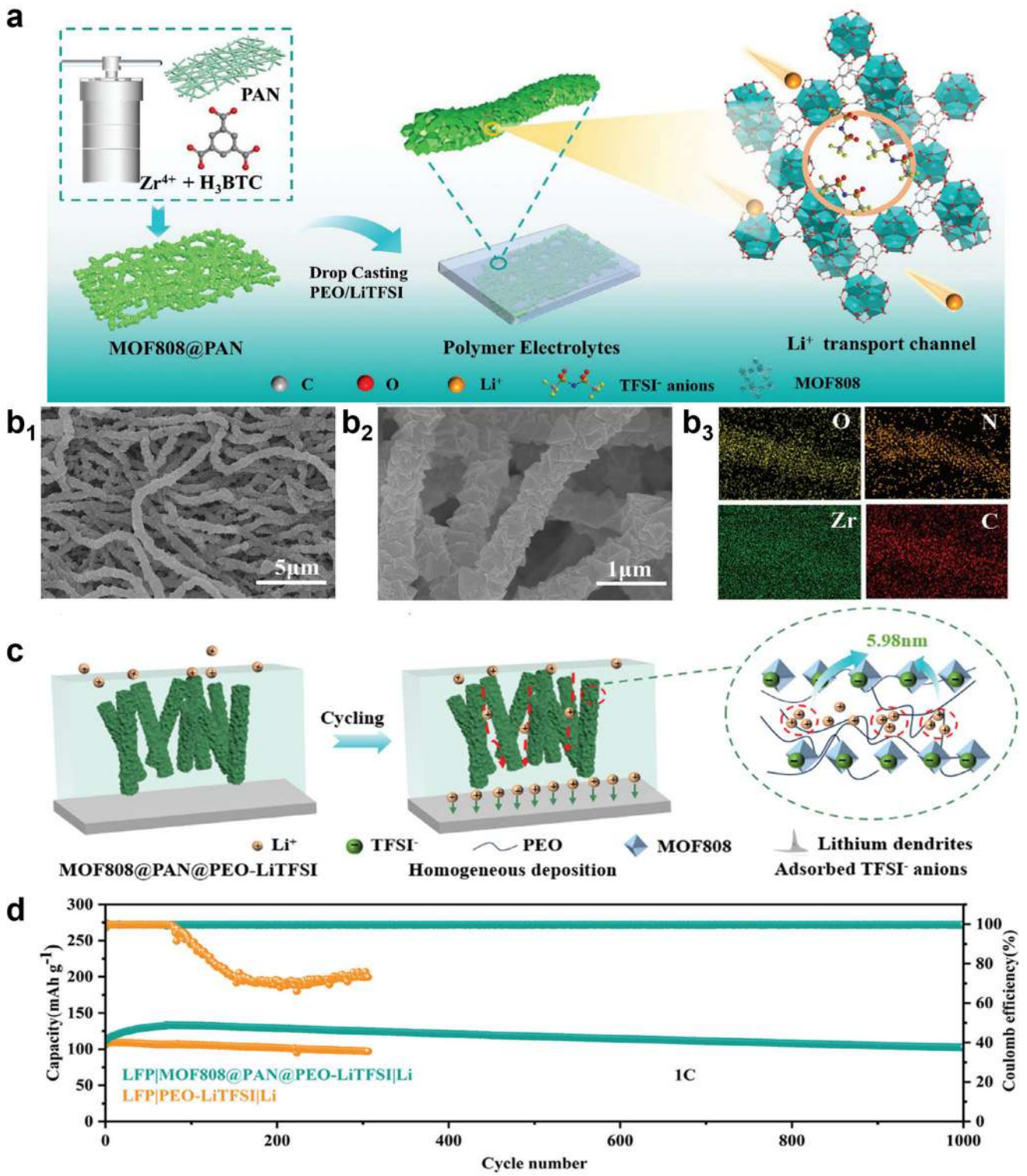

Fig. 9 **a** Schematic of the in situ hydrothermal growth of MOF808 on PAN fiber. $\mathbf{b_1}$–$\mathbf{b_2}$ Morphology of MOF808 network on loaded PAN fiber at different magnifications. $\mathbf{b_3}$ EDS spectra of MOF808@PAN. **c** Schematic diagram of uniform Li^+ deposition as well as continuous transport path before and after cycling of MOF808@PAN@PEO–LiTFSI polymer electrolyte, MOFS808@PAN@PEO–LiTFSI polymer electrolyte cycling process, MOFS808 adsorbs anions to regulate the Li^+ flux concentration, increasing the localized Li^+ flux concentration. **d** Cycling performance of LFP/PEO–LiTFSI/Li and LFP/MOFs808@PAN@PEO–LiTFSI/Li batteries at 60 °C. Reproduced with permission [97]. Copyright 2025, Wiley–VCH

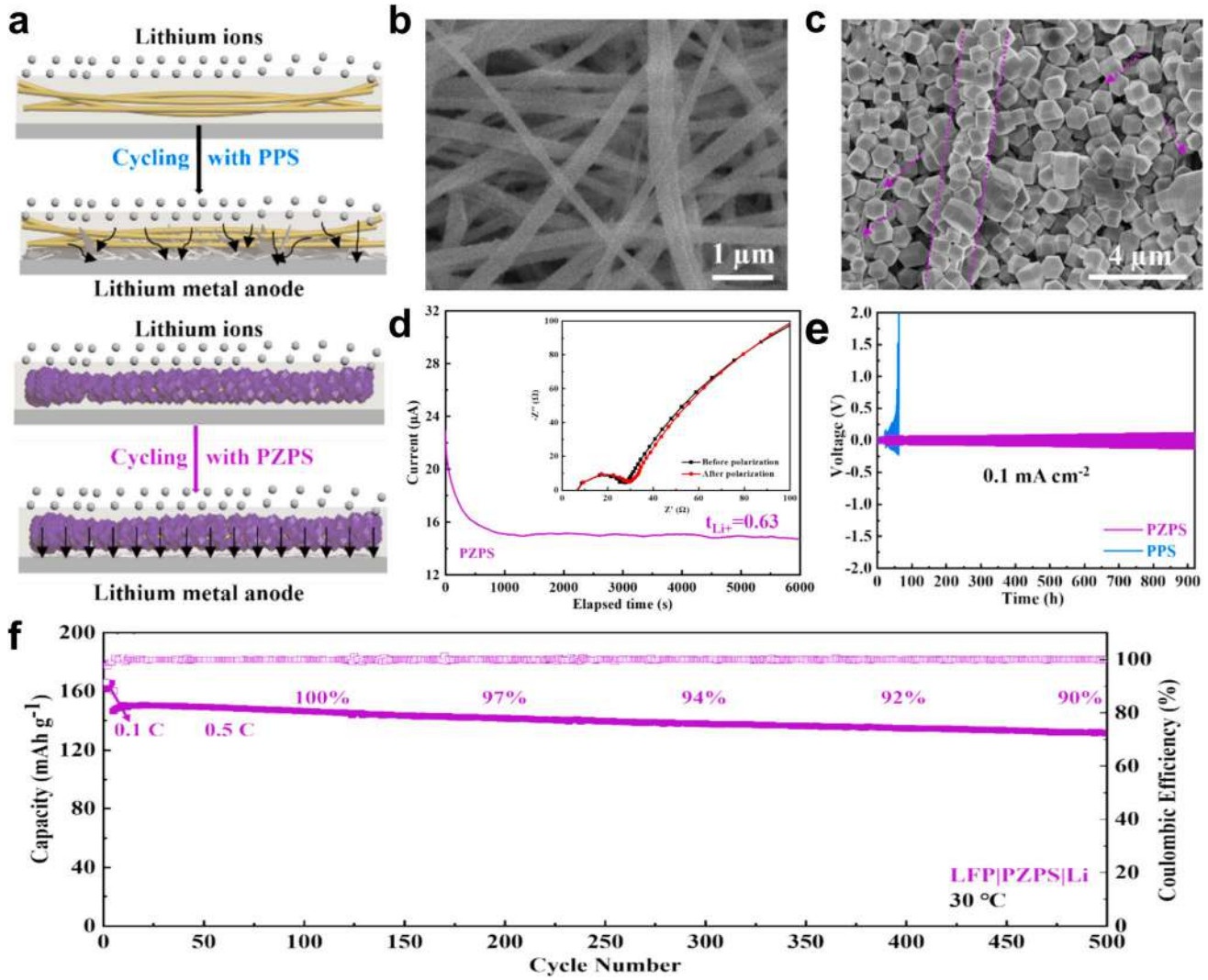

Fig. 10 **a** The schematic illustration of the mechanism for improved interfacial stability between PZPS (PVDF-HFP/2-MI@ZIF-67 + PEGDA/SN/LiTFSI) and Li metal anode. **b–c** Surface SEM images of PVDF-HFP/2-MI and PVDF-HFP/2-MI@ZIF-67. **d** Polarization curves and the corresponding Nyquist plots before and after polarization for PZPS. **e** The time-dependent voltage profiles of Li/PPS/Li and Li/PZPS/Li cells at a current density of 0.1 mA cm^{-2} at 30 °C; PPS refers to PVDF-HFP/2-MI + PEGDA/SN/LiTFSI. **f** Cycling performance of LFP/PZPS/Li batteries at 30 °C and 0.5 C, loading was 1 mg cm^{-2}. Reproduced with permission [87]. Copyright 2024, Elsevier

blending methods. Furthermore, the vertical growth of MOFs along the nanofiber surfaces creates continuous ion transport channels, enabling rapid radial Li^+ migration and consequently improving both ionic conductivity and t_{Li}^+. This core–shell configuration simultaneously preserves the inherent flexibility of the polymer framework while substantially reinforcing mechanical strength through the MOFs coating, thereby effectively suppressing lithium dendrite penetration. Research further indicates that precise control over MOFs growth density and orientation on nanofiber surfaces can optimize ion transport kinetics and interfacial stability, offering a promising materials design paradigm for developing high-safety and high-energy-density SSLMBs.

3.3 Functionalization of MOFs/Polymer Nanofiber Electrolytes

To improve the mechanical properties of the fiber skeleton, researchers can also optimize the fiber. He et al. [98] constructed a compact composite solid-state electrolyte featuring a 3D continuous Li^+ transport network by coupling a thermally treated PAN nanofiber network with a MOFs coating

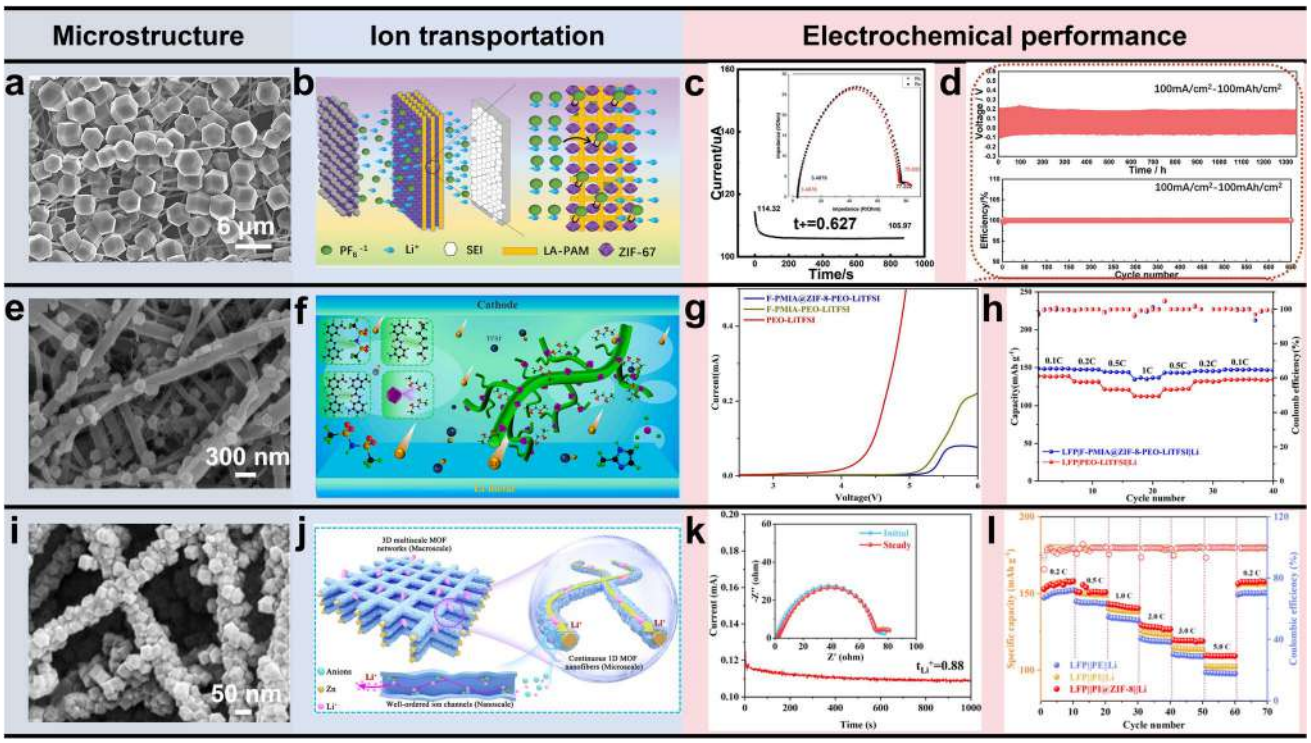

Fig. 11 **a** The surface and cross-section morphology of ZIF-67-LA-PAM. **b** The schematic diagram of ion transport mechanism of ZIF-67-LA-PAM electrolyte. **c** Lithium-ion transfer number of the ZIF-67-LA-PAM. **d** Symmetrical Li cells of ZIF-67-LA-PAM at 100 mA cm^{-2}@100 mAh cm^{-2} at 30 °C. Reproduced with permission [62]. Copyright 2022, Wiley–VCH. **e** The surface and cross-section morphology of F-PMIA@ZIF-8. **f** Mechanism for enhanced Li^+ transport by F-PMIA@ZIF-8. **g** The electrochemical window of different types of polymer electrolytes using linear scanning voltammetry (LSV). **h** The rate performance of LFP/Li battery at 50 °C. Reproduced with permission [110]. Copyright 2023, Elsevier. **i** The surface morphology and EDS mappings of PI@ZIF-8 nanofiber separators. **j** Schematic illustration for the 3D multiscale MOF networks enabling continuous and high-efficiency Li^+ transport. **k** Current–time curves and the relevant Nyquist plots of PI@ZIF-8 nanofiber separators in symmetric Li/Li cells. **l** Rate performance at a sulfur loading of 4.5 mg cm^{-2}. Reproduced with permission [111]. Copyright 2025, Royal Society of Chemistry

layer (denoted as h-PAN@MOFs in Fig. 12a). Interconnected MOFs are uniformly deposited on heat-treated h-PAN nanofibers, preserving their cross-linked morphology with an average diameter of approximately 200 nm. (Fig. 12b–c). This engineered architecture established high-efficiency Li^+ transport channels and networks, achieving a high ionic conductivity of 1.03×10^{-3} S cm^{-1} (Fig. 12e). The MOFs-dependent Li^+ coordination environment further facilitated the formation of a stable interfacial layer (Fig. 12f). The h-PAN@MOFs network also imparted high tensile strength (20.84 MPa) to the compact electrolyte (Fig. 12d). A Li/NCM811 cell employing the h-PAN@MOFs electrolyte delivers a capacity retention of 85.7% after 190 cycles at 0.5 C with the 4.5 mg cm^{-2} cathode (Fig. 12g). This work provides a straightforward strategy for modulating the Li^+ coordination state and its spatial distribution within solid electrolytes for fast-charging solid-state lithium metal batteries.

In addition, MOFs are a class of inorganic–organic hybrid materials that often exhibit inherent brittleness, high cost, poor processability, and limited scalability. To enhance the mechanical strength of composite electrolyte membranes, Tong et al. [101] successfully fabricated a flexible and stretchable nanofibrous membrane composed of a crystalline COFs (TPPA-1) via electrospinning and a polymer sacrificial template strategy (Fig. 12h). This nanofibrous membrane serves as a porous support for the composite system, offering not only excellent flexibility and stretchability but also providing abundant pores for subsequent MOFs growth. Thereafter, a polycrystalline selective layer was constructed through the tailored and confined growth of ZIF-8 on the surface of the COFs membrane and within the inter-fiber voids. As a MOFs material with exceptional molecular sieving capability, ZIF-8 interweaves with the COFs nanofibers, forming an interpenetrating network structure that constitutes a mutually supportive intergrown layer. A distinctive feature of this COFs/MOFs composite membrane lies in the highly stable interface between the two crystalline porous materials, achieved through their chemical similarity. This stability enables the composite membrane to operate under hydraulic pressure for extended durations

without compaction, thereby ensuring long-term durability and reliability in practical applications.

4 Electrospun MOFs/Polymer Composite for Other Batteries

Sodium-based batteries, leveraging the abundance of sodium resources, have emerged as a promising alternative to lithium-ion batteries [125, 126]. Electrospun MOFs/polymer composites have emerged as promising functional materials for advancing sodium metal batteries (SMBs), offering enhanced ionic conductivity, mechanical stability, and interfacial control to address key challenges, such as dendrite growth and electrolyte degradation [127]. A typical example is Tian et al. [128] reported PPNM (PEO + PAN@Cu-MOF with a 3D interconnected Cu-MOFs on PAN fibers in PEO-based solid polymer electrolytes (SPEs), which achieves high-performance sodium metal batteries through competitive coordination and dual interphase regulation, enabling excellent cycling stability and rate capability (Fig. 13a). This team proposed a competitive coordination mechanism that elucidates the local coordination environment within PEO-based SPEs. Specifically, in addition to Na^+, the open metal sites (OMS) of Cu-MOFs also actively participate in the coordination of $TFSI^-$ (Fig. 13d). Therefore, the assembled full cells with various cathodes demonstrate excellent rate capability and cycling stability. In particular, the NVP@C/PPNM/Na cell maintains 90.06% capacity retention after 2000 cycles at 200 mA g^{-1} in Fig. 13b–c. Figure 13e illustrates a comparison of the performance of different SSEs. The battery with the PPNM electrolyte exhibits superior performance, surpassing most previously reported sodium metal solid-state batteries, further indicating its great potential for future applications in SMBs.

5 Conclusions and Perspectives

Based on the comprehensive analysis presented in this review, electrospinning technology has emerged as a highly promising method for developing advanced solid-state electrolytes in next-generation lithium metal batteries. This review has systematically evaluated two main integration strategies, which are the incorporation of MOFs in polymer nanofiber and the in situ growth of MOFs on polymer nanofiber. Each strategy exhibits distinct structural characteristics and corresponding lithium-ion transport mechanisms. In the first approach where MOFs are incorporated in polymer nanofiber, MOFs become encapsulated inside the polymer nanofibers. The primary ion transport mechanism involves migration through the continuous polymer phase, supplemented by hopping conduction at the interfaces between the polymer and MOFs. Although some ions might theoretically migrate through the internal pores of the MOFs, this pathway generally remains discontinuous due to the random dispersion and unfavorable orientation of the MOF fillers. In contrast, the in situ growth strategy enables MOFs to form continuous and oriented crystalline layers that either coat the nanofiber surfaces or bridge adjacent nanofibers, creating well-interconnected porous channels. This configuration supports ion transport mainly through high-flux diffusion within the intrinsic pores of the MOFs, further enhanced by surface functional group-mediated migration. This structurally superior arrangement generally results in more continuous and ordered transport pathways, leading to enhanced conduction efficiency. Over the past five years, the integration of MOFs with electrospun polymer matrices, particularly through advanced processes such as in situ polymerization, has significantly improved the mechanical strength, interfacial compatibility, and ionic conductivity of electrolytes. These enhancements originate from the synergistic combination of the rigid, ordered porous structure of MOFs that provides continuous ion transport channels, together with the flexible and electrochemically stable polymer matrix.

Looking forward, several critical challenges require focused attention to advance MOFs/polymer nanofiber electrolytes. First, the continued reliance on conventional organic solvents compromises both safety profiles and environmental sustainability. Currently, there is a lack of precise quantitative data on residual solvents in the field, which constitutes a noteworthy research gap. Second, the interfacial interactions between MOFs and polymers need further optimization to achieve enhanced compatibility and performance. Additionally, systematic investigation into the design principles and compatibility of multi-component polymer systems remains an important unmet need. To realize the crucial performance targets of room-temperature ionic conductivity exceeding 3 mS cm^{-1} coupled with electrochemical stability windows beyond 5 V, future efforts should prioritize addressing these fundamental limitations through coordinated materials design and processing innovations. Through targeted advancements in these areas, MOFs/polymer nanofiber electrolytes are positioned to overcome current barriers and pave the way for next-generation energy storage technologies (Fig. 14).

Future studies should prioritize the following strategic directions to advance the development of electrospun MOFs/polymer nanofiber electrolytes:

1. Green solvent system development: The replacement of conventional organic solvents with non-flammable, low-toxicity alternatives, such as deep eutectic solvents (DES) and polymeric ionic liquids, represents a critical pathway toward safer electrolytes. Guided by compu-

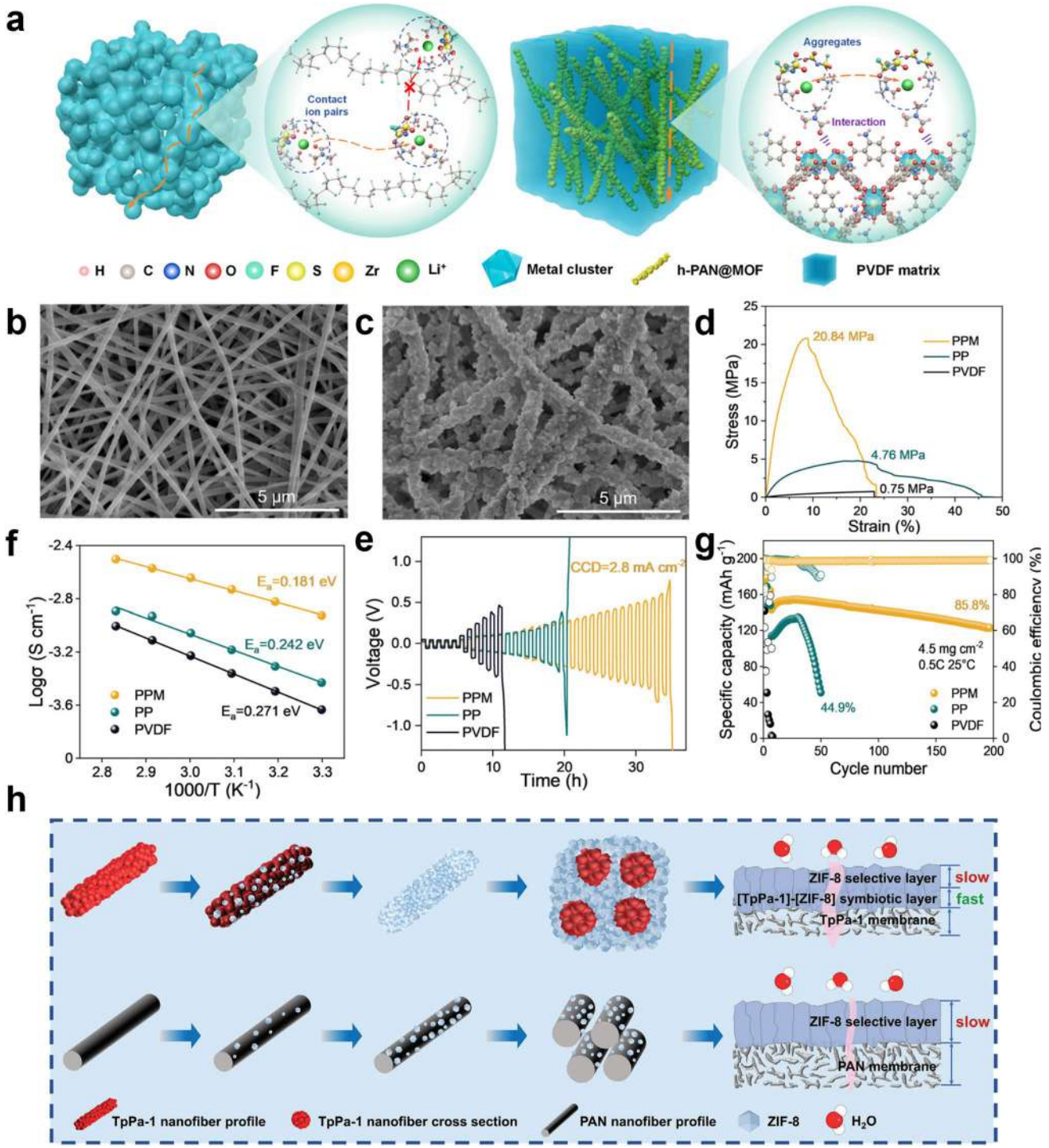

Fig. 12 Characteristics of heat-treated PAN fiber networks, PVDF, and PPM (PVDF + h-PAN@UIO-66-NH_2) electrolytes. **a** Schematic of the ion transport and solvation structure modes in PVDF electrolytes and PPM electrolytes, SEM images of **b** h-PAN nanofibers and **c** h-PAN@MOFs networks (h refers heat-treated). **d** Stress–strain curves of PPM, PP (PVDF + h-PAN) and PVDF. **e** Arrhenius plots of ionic conductivity of electrolytes. **f** Critical current density (CCD) of the Li/Li symmetric cells. **g** Long-term cycling stability of Li/PPM/NCM811 cells with different electrolytes at 25 °C. Reproduced with permission [98]. Copyright 2024, Wiley–VCH. The formation process of micromorphology of the COF–MOFs composite membrane. **h** Schematic illustration of the confined growth of ZIF-8 in the gaps between the TpPa-1 (A self-standing pristine COF) and PAN nanofibers. Reproduced with permission [101]. Copyright 2024, Royal Society of Chemistry

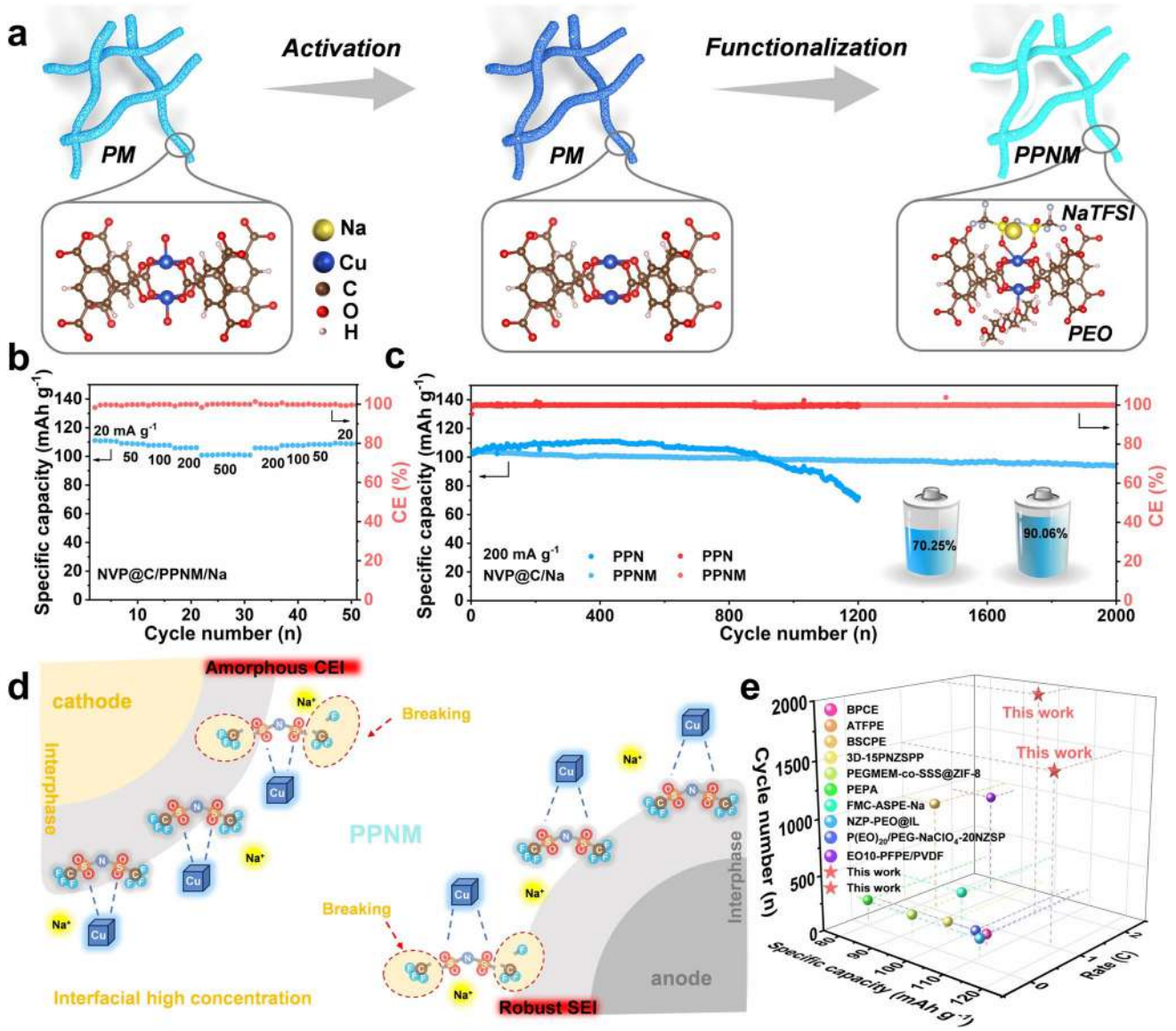

Fig. 13 **a** Schematic diagram of the synthesis and coordination structure of PPNM (PEO + PAN@Cu-MOF) electrolyte. **b** Rate performance and **c** cycling performance of NVP@C/PPN (PEO + PAN)/Na and NVP@C/PPNM/Na at 200 mA g^{-1} and 30 °C ($NVP@C = Na_3V_2(PO_4)_3@C$, mass loading: ca. 1.5–2 mg cm^{-2}). **d** Schematic diagram of dual interphase regulation. **e** Comparison of different SSEs. Reproduced with permission [128]. Copyright 2025, Wiley–VCH

tational screening, customized solvents exhibiting high lithium salt solubility, low viscosity, and wide electrochemical windows should be designed. These systems can regulate Li^+ solvation structures through confinement within MOFs channels while simultaneously plasticizing the polymer matrix to enhance chain mobility. A fundamental understanding of their interfacial adsorption and reaction mechanisms will further promote the formation of inorganic-rich, stable interphases, thereby suppressing dendrite growth and side reactions.

2. Advanced composite strategy optimization: Promoting the research progress by implementing multiscale interface engineering. Specific approaches include MOFs surface functionalization with targeted groups (–SO_3H, –NH_2, or fluorinated chains) to enhance interfacial compatibility and facilitate lithium salt dissociation. Concurrently, molecular-level engineering of polymer through tailored architectures, such as star-shaped or hyperbranched topologies integrated with crown ether or ionic liquid motifs, can amplify synergistic effects with the surfaces and channels of MOFs. Furthermore, robust interfacial bonding strategies via covalent grafting or coordination interactions should be developed to construct durable molecular bond effectively mitigat-

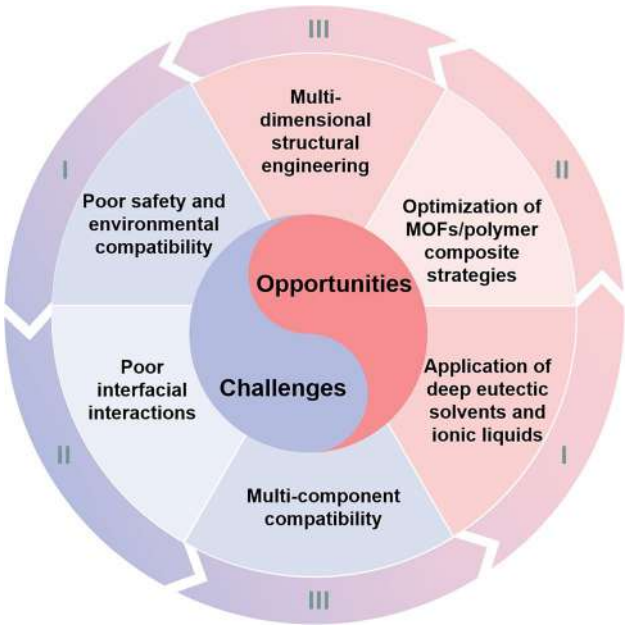

Fig. 14 Schematic illustration of challenges and prospective strategies for MOFs/polymer nanofiber electrolytes via electrospinning

ing phase separation and preserving structural integrity under extended cycling.

3. Multidimensional structural engineering: Electrospinning enables the construction of 3D interconnected MOFs/polymer nanofiber networks with tunable diameter, orientation, and porosity, significantly reducing ion transport tortuosity. Through techniques, such as electric-field alignment, template confinement, or microfluidic processing, MOFs can be oriented along nanofiber axial and radial to form continuous fast ion transportation. At the macroscopic scale, hierarchical designs incorporating gradient pores or biomimetic channel structures allow spatial regulation of ion flux. By synergistically utilizing MOFs microporosity and inter-fiber mesoporosity, such multidimensional designs facilitate simultaneous achievement of high ionic conductivity, superior Li^+ transference number, and robust mechanical properties.

Future studies should prioritize understanding the coupling effects between the microstructure of electrospun nanofibers and MOFs functionalization on ionic transport mechanisms. Advanced in situ characterization techniques, integrated with multiscale simulations, are critically needed to elucidate ion migration pathways and interfacial kinetics at both MOFs/polymer and electrode–electrolyte interfaces. Particular emphasis should be placed on decoupling the individual contributions of MOFs chemistry and nanofiber morphology to Li^+ transport behavior. Such fundamental insights will accelerate the rational design of high-performance electrolytes and facilitate their deployment in higher-energy-density battery systems and a broader range of electrochemical devices.

Supplementary Information The online version contains supplementary material available at https://doi.org/10.1007/s42765-026-00692-4.

Acknowledgements This work was supported by the Fundamental Research Funds for the Central Universities (No. 2682024CX059), Start-up Research Funding of Southwest Jiaotong University (No. 2682024KJ003), Postdoctoral Fellowship Program of China Postdoctoral Science Foundation (No. GZC20241407), and Sichuan Science and Technology Program (No. 2025ZNSFSC1413).

Author Contributions X. G., L. G., and P. D. contributed equally to this work. X. G. and L. G. prepared the draft of this work. X. Z., X. J., G. F., C. X., S. Y., J. Z., and M.-K. S. revised this work. P. D and W. Y. supervised and revised this work.

Declarations

Conflict of interest The authors declare that they have no known competing financial interests or personal relationships that could have appeared to influence the work reported in this paper.

References

1. Akyüz ES, Telli E, Farsak M. Hydrogen generation electrolyzers: paving the way for sustainable energy. *Int J Hydrogen Energy*. **2024**;*81*: 1338.
2. Ghosh S, Sibi A, Priyanga GS, Dagdia ZC, Thomas T. Temperature-dependent performance prediction for cerium oxynitride solid-state symmetric supercapacitor using machine learning. *J Energy Storage*. **2025**;*113*: 115562.
3. Park J, Lim JH, Kang JH, Lim J, Jang HW, Shin H, Park SH. A review of understanding electrocatalytic reactions in energy conversion and energy storage systems via scanning electrochemical microscopy. *J Energy Chem*. **2023**;*91*: 155.
4. Xia S, Yang C, Jiang Z, Fan W, Yuan T, Pang Y, Sun H, Chen T, Li X, Zheng S. Towards practical lithium metal batteries with composite scaffolded lithium metal: an overview. *Adv Compos Hybrid Mater*. **2023**;*23*: 769.
5. Jin Y, Lee IH, Gu T, Jung SH, Chang H, Kim BS, Moon J, Whang D. Vertically aligned conductive metal–organic-frameworks with switchable electrical conductivity for Li metal anode. *Adv Funct Mater*. **2024**;*34*: 10097.
6. Li S, Chen Y, Li C, Ko TJ. Potent anionophilic bimetallic frameworks enabling lithium dendrite-free deposition for high-performance lithium batteries. *Energy Storage Mater*. **2025**;*80*: 104444.
7. Zhang X, Yu H, Ben L, Cen G, Sun Y, Wang L, Hao J, Zhu J, Sun Q, Qiao R, Yao X, Zhang H, Huang X. Topology fortified anodes powered high-energy all-solid-state lithium batteries. *Adv Mater*. **2025**;*37*: 6298.
8. Jaumaux P, Wu J, Shanmukaraj D, Wang Y, Zhou D, Sun B, Kang F, Li B, Armand M, Wang G. Non-flammable liquid and quasi-solid electrolytes toward highly-safe alkali metal-based batteries. *Adv Funct Mater*. **2020**;*31*: 202008644.
9. Zhu GR, Zhang Q, Liu QS, Bai QY, Quan YZ, Gao Y, Wu G, Wang YZ. Non-flammable solvent-free liquid polymer electrolyte for lithium metal batteries. *Nat Commun*. **2023**;*14*: 4617.

10. Liu Z, Chen S, Shi Z, Qiu P, He K, Lu Q, Yu M, Liu T. Multivalent dipole interactions-driven supramolecular polymer layer enables highly stable Zn anode under harsh conditions. *Adv Energy Mater*. **2025**;*15*: 2502010.
11. Wang M, Wu Y, Qiu M, Li X, Li C, Li R, He J, Lin G, Qian Q, Wen Z, Li X, Wang Z, Chen Q, Chen Q, Lee J, Mai YW, Chen Y. Research progress in electrospinning engineering for all-solid-state electrolytes of lithium metal batteries. *J Energy Chem*. **2021**;*61*:253.
12. Ren Y, Chen S, Odziomek M, Guo J, Xu P, Xie H, Tian Z, Antonietti M, Liu T. Mixing functionality in polymer electrolytes: a new horizon for achieving high-performance all-solid-state lithium metal batteries. *Angew Chem Int Ed*. **2025**;*64*: e202422169.
13. Hu JK, Gao YC, Yang SJ, Wang XL, Chen X, Liao YL, Li S, Liu J, Yuan H, Huang JQ. High energy density solid-state lithium metal batteries enabled by in situ polymerized integrated ultrathin solid electrolyte/cathode. *Adv Funct Mater*. **2024**;*34*:11633.
14. Wang Y, Huang T, Li C, Zhang X, Xia S. Current progress and future perspectives of inorganic/organic composite solid electrolytes for solid-state lithium metal batteries. *Mater Sci Eng B*. **2025**;*318*: 118316.
15. Zheng C, Lu Y, Chang Q, Song Z, Xiu T, Jin J, Badding ME, Wen Z. High-performance garnet-type solid-state lithium metal batteries enabled by scalable elastic and Li^+-conducting interlayer. *Adv Funct Mater*. **2023**;*33*: 202302729.
16. Huang X, Pan L, Gao M, Cao M, Wang Y, Ling Y, Ke X, Yuan P, Wang T, Xiao R, Li T. Biomass-based solid-state electrolyte: an emerging material toward high-performance and sustainable solid-state batteries. *Mater Today*. **2025**;*90*:996.
17. Liu XX, Pan L, Zhang H, Liu C, Cao M, Gao M, Zhang Y, Xu Z, Wang Y, Sun Z. Indium-MOF as multifunctional promoter to remove ionic conductivity and electrochemical stability constraints on fluoropolymer electrolytes for all-solid-state lithium metal battery. *Nano-Micro Lett*. **2025**;*17*: 249.
18. Pan L, Sun S, Yu G, Liu XX, Feng S, Zhang W, Turgunov M, Wang Y, Sun Z. Stabilizing solid electrolyte/Li interface via polymer-in-salt artificial protection layer for high-rate and stable lithium metal batteries. *Chem Eng J*. **2022**;*449*: 137682.
19. Wang Y, Yuan P, Liu XX, Feng S, Cao M, Ding J, Liu J, Kure-Chu SZ, Hihara T, Pan L, Sun Z. Sacrificial NH_4HCO_3 inhibits fluoropolymer/garnet interfacial reactions toward 1ms cm^{-1} and 5v-level composite solid electrolyte. *Adv Funct Mater*. **2024**;*34*: 2405060.
20. Wang H, Duan S, Zheng Y, Qian L, Liao C, Dong L, Guo H, Ma C, Yan W, Zhang J. Solid-state electrolytes based on metal-organic frameworks for enabling high-performance lithium-metal batteries: fundamentals, progress, and perspectives. *Etransportation*. **2024**;*20*: 100311.
21. Yang SJ, Hu JK, Jiang FN, Yuan H, Park HS, Huang JQ. Safer solid-state lithium metal batteries: mechanisms and strategies. *InfoMat*. **2023**;*6*: 12512.
22. Ahmadijokani F, Molavi H, Bahi A, Fernández R, Alaee P, Wu S, Wuttke S, Ko F, Arjmand M. Metal-organic frameworks and electrospinning: a happy marriage for wastewater treatment. *Adv Funct Mater*. **2022**;*32*: 7723.
23. Wang Y, Liu Z, Zhao Z, Fei M, Xie Y, Guo H, Zhao P, Fei J. Modulation of metal centers of MOF in-situ grown on lignin-derived carbon to enhance adsorption capacity and electrochemical sensing performance for bisphenol A. *Chem Eng J*. **2024**;*499*: 156279.
24. Zhou Y, Abazari R, Chen J, Tahir M, Kumar A, Ikreedeegh RR, Rani E, Singh H, Kirillov AM. Bimetallic metal–organic frameworks and MOF-derived composites: recent progress on electro- and photoelectrocatalytic applications. *Coord Chem Rev*. **2021**;*451*: 214264.
25. Duan S, Qian L, Zheng Y, Zhu Y, Liu X, Dong L, Yan W, Zhang J. Mechanisms of the accelerated Li^+ conduction in MOF-based solid-state polymer electrolytes for all-solid-state lithium metal batteries. *Adv Mater*. **2024**;*36*: 2314120.
26. Dong P, Zhang X, Hiscox W, Liu J, Zamora J, Li X, Su M, Zhang Q, Guo X, McCloy J, Song MK. Toward high-performance metal–organic-framework-based quasi-solid-state electrolytes: tunable structures and electrochemical properties. *Adv Mater*. **2023**;*35*: 11841.
27. He H, Deng N, Wang X, Gao L, Tang C, Wu E, Ren J, Yang X, Feng N, Gao D, Zhuang X. Design strategies, characterization mechanisms, and applications of MOFs in polymer composite electrolytes for solid-state lithium metal batteries. *Adv Funct Mater*. **2025**;*35*: 21670.
28. Li B, Wang C, Yu R, Han J, Jiang S, Zhang C, He S. Recent progress on metal–organic-framework/polymer composite electrolytes for solid-state lithium metal batteries: Ion transport regulation and interface engineering. *Energy Environ Sci*. **2024**;*17*: e02705.
29. Lu G, Meng G, Liu Q, Feng L, Luo J, Liu X, Luo Y, Chu PK. Advanced strategies for solid electrolyte interface design with mof materials. *Adv Powder Mater*. **2023**;*3*: 100154.
30. Yang B, Shi Y, Kang DJ, Chen Z, Pang H. Architectural design and electrochemical performance of MOF-based solid-state electrolytes for high-performance secondary batteries. *Interdiscip Mater*. **2023**;*2*: 12108.
31. Ren Z, Li J, Gong Y, Shi C, Liang J, Li Y, He C, Zhang Q, Ren X. Insight into the integration way of ceramic solid-state electrolyte fillers in the composite electrolyte for high performance solid-state lithium metal battery. *Energy Storage Mater*. **2022**;*51*:130.
32. Yu W, Liu Z, Xiang H, Feng X, Duan W, Cheng B, Li G, Deng N, Kang W. Resilience-driven 3D quasi-vertical fiber networks in composite electrolyte for fast ion-conduction and stress self-adaptation in all-solid-state batteries. *Energy Storage Mater*. **2025**;*80*: 104403.
33. Li Q, Bai M, Wang X, Li J, Lin X, Shao S, Li D, Wang Z. A MOF@$ZnIn_2S_4$ composite quasi-solid electrolyte for highly reversible Zn-ion batteries. *Adv Funct Mater*. **2025**;*35*: 2344.
34. Liu S, Zhou L, Zhong T, Wu X, Neyts K. Sulfide/polymer composite solid-state electrolytes for all-solid-state lithium batteries. *Adv Energy Mater*. **2024**;*14*: 202403602.
35. Chen Q, Ouyang C, Liang Y, Liu H, Duan H. Composite polymer electrolyte with vertically aligned garnet scaffolds for quasi solid-state lithium batteries. *Energy Storage Mater*. **2024**;*69*: 103418.
36. Tong RA, Huang Y, Feng C, Dong Y, Wang CA. In-situ polymerization confined pegdme-based composite quasi-solid-state electrolytes for lithium metal batteries. *Adv Funct Mater*. **2024**;*34*: 15777.
37. Yang H, Zhang B, Jing M, Shen X, Wang L, Xu H, Yan X, He X. In situ catalytic polymerization of a highly homogeneous pdol composite electrolyte for long-cycle high-voltage solid-state lithium batteries. *Adv Energy Mater*. **2022**;*12*: 2201762.
38. Chen C, Zhang W, Zhu H, Li B, Lu Y, Zhu S. Fabrication of metal-organic framework-based nanofibrous separator via one-pot electrospinning strategy. *Nano Res*. **2020**;*14*: 14465.
39. Graham SA, Kurakula A, Kavarthapu VS, Lee JK, Manchi P, Paranjape MV, Yu JS. Metal–organic framework embedded electrospun fibrous membranes-based hybrid nanogenerators with hierarchical modified polyamide films for mechanical energy harvesting and iot applications. *Adv Funct Mater*. **2025**;*4*: e07125.
40. Liu X, Pan L, Zhang H, Yuan P, Cao M, Wang Y, Xu Z, Gao M, Sun Z. Host-guest inversion engineering induced superionic composite solid electrolytes for high-rate solid-state alkali metal batteries. *Nano-Micro Lett*. **2025**;*17*: 190.

41. Pan L, Feng S, Sun H, Liu XX, Yuan P, Cao M, Gao M, Wang Y, Sun Z. Ultrathin, mechanically durable, and scalable polymer-in-salt solid electrolyte for high-rate lithium metal batteries. *Small*. **2024**;*20*: 2400272.
42. Centrone A, Yang Y, Speakman S, Bromberg L, Rutledge GC, Hatton TA. Growth of metal−organic frameworks on polymer surfaces. *J Am Chem Soc*. **2010**;*132*:15687.
43. Jia H, Liu K, Lam Y, Tawiah B, Xin JH, Nie W, Jiang SX. Fiber-based materials for aqueous zinc ion batteries. *Adv Fiber Mater*. **2023**;*5*:36.
44. Liu X, Zhang Y, Guo X, Pang H. Electrospun metal–organic framework nanofiber membranes for energy storage and environmental protection. *Adv Fiber Mater*. **2022**;*4*:1463.
45. Liu Y, Huang J, Huang H, Yu P, Ji J, Li L, Huang J. Electrospinning engineering for aqueous zinc-ion batteries: from multi-scale structural regulation to energy storage performance enhancement. *Adv Fiber Mater*. **2025**;*25*: 42765.
46. Shi F, Chen C, Xu ZL. Recent advances on electrospun nanofiber materials for post-lithium ion batteries. *Adv Fiber Mater*. **2021**;*3*:275.
47. Wu S, Wang C, Tang Y, Jiang J, Jiang H, Xu X, Cui B, Jiang Y, Wang Y. Metal–organic framework-derived hierarchical Cu_9S_5/C nanocomposite fibers for enhanced electromagnetic wave absorption. *Adv Fiber Mater*. **2024**;*6*:430.
48. Bian Y, Wang S, Jin D, Wang R, Chen C, Zhang L. A general anion exchange strategy to transform metal-organic framework embedded nanofibers into high-performance lithium-ion capacitors. *Nano Energy*. **2020**;*75*: 104935.
49. Lin P, Lu X, Deka BJ, Shang J, Wu H, Sun J, Yi C, Farid MU, An AK, Guo J. Research progress in the preparation of electrospinning MOF nanofiber membranes and applications in the field of photocatalysis. *Sep Purif Technol*. **2024**;*356*: 129948.
50. Liu S, Yan Y, Zhang S, Yan D, Cai Y, Yin S, Lu Q, Ren W, Zhang Q, Xing Y. A 3D interconnected functionalized metal organic framework-reinforced solid electrolyte by in-situ polymerization for stable lithium metal battery. *Energy Storage Mater*. **2025**;*80*: 104396.
51. Liu X, Zhang Y, Guo X, Pang H. Electrospun metal–organic framework nanofiber membranes for energy storage and environmental protection. *Adv Fiber Mater*. **2022**;*4*: 1463.
52. Sankar SS, Karthick K, Sangeetha K, Karmakar A, Madhu R, Kundu S. Current perspectives on 3D ZIFs incorporated with 1D carbon matrices as fibers via electrospinning processes towards electrocatalytic water splitting: a review. *J Mater Chem A*. **2021**;*9*: 11961.
53. Son HB, Cho S, Baek K, Jung J, Nam S, Han DY, Kang SJ, Moon HR, Park S. All-impurities scavenging, safe separators with functional metal–organic-frameworks for high-energy-density Li-ion battery. *Adv Funct Mater*. **2023**;*33*: 2563.
54. UcakAstarlioglu MG, Fernando PUAI, Spane SA, Rodriguez SA, Kosgei GK, Weiss CA, Beckman IP, Villacorta B, Nouranian S, AlOstaz A. FIMOFs: fiber-integrated metal–organic frameworks through electrospinning. *Polymers*. **2025**;*17*: 1106.
55. Wang R, Fu R, Wang C, Wang J, Peng R, Zhu X, Yan X, Kang H, Mao Y, Kim M, Yamauchi Y. Sustainable application of MOF electrospinning in the environment. *J Environ Chem Eng*. **2025**;*13*: 117022.
56. Ding C, Du Y, Fischer T, Timm J, Marschall R, Senker J, Agarwal S. Liquid–liquid–solid interfacial polymerization approach to rapid fabrication of large-sized, self-standing structured COF membranes. *J Mater Chem A*. **2025**;*13*: 20688.
57. Man P, He B, Zhang Q, Zhou Z, Li C, Li Q, Wei L, Yao Y. A one-dimensional channel self-standing mof cathode for ultra-high-energy-density flexible Ni–Zn batteries. *J Mater Chem A*. **2019**;*7*: 27217.
58. Yu J, Cai D, Si J, Zhan H, Wang Q. MOF-derived $NiCo_2S_4$ and carbon hybrid hollow spheres compactly concatenated by electrospun carbon nanofibers as self-standing electrodes for aqueous alkaline zn batteries. *J Mater Chem A*. **2022**;*10*: 4100.
59. Zhang C, Shen L, Shen JQ, Liu F, Chen G, Tao R, Ma SX, Peng YT, Lu YF. Anion-sorbent composite separators for high-rate lithium-ion batteries. *Adv Mater*. **2019**;*31*: e1808338.
60. Zhou C, He Q, Li Z, Meng J, Hong X, Li Y, Zhao Y, Xu X, Mai L. A robust electrospun separator modified with in situ grown metal-organic frameworks for lithium-sulfur batteries. *Chem Eng J*. **2020**;*395*: 124979.
61. Yang LY, Cao JH, Cai BR, Liang T, Wu DY. Electrospun MOF/PAN composite separator with superior electrochemical performances for high energy density lithium batteries. *Electrochim Acta*. **2021**;*382*: 138346.
62. Guan J, Feng X, Zeng Q, Li Z, Liu Y, Chen A, Wang H, Cui W, Liu W, Zhang L. A new in situ prepared MOF-natural polymer composite electrolyte for solid lithium metal batteries with superior high-rate capability and long-term cycling stability at ultrahigh current density. *Adv Sci*. **2022**;*10*: 3916.
63. Yu W, Shen L, Lu X, Han J, Geng N, Lai C, Xu Q, Peng Y, Min Y, Lu Y. Novel composite separators based on heterometallic metal–organic-frameworks improve the performance of lithium-ion batteries. *Adv Energy Mater*. **2023**;*13*: 202204055.
64. Liu L, Zhu L, Wang Y, Guan X, Zhang Z, Li H, Wang F, Zhang H, Zhang Z, Yang Z, Ma T. Starfish-inspired solid-state Li-ion conductive membrane with balanced rigidity and flexibility for ultrastable lithium metal batteries. *Angew Chem Int Ed*. **2024**;*64*: 20001.
65. Lin R, Jin Y, Li Y, Fu M, Gong Y, Lei L, Zhang Y, Xu J, Xiong Y. Decoupling interfacial stability and ion transport in solid polymer electrolyte by tailored ligand chemistry for lithium metal battery. *Adv Funct Mater*. **2024**;*35*: 21880.
66. Cho YJ, Beak JW, Sagong M, Ahn S, Nam JS, Kim ID. Electrospinning and nanofiber technology: fundamentals, innovations, and applications. *Adv Mater*. **2025**;*37*: 202500162.
67. Chen Y, Dong X, Shafiq M, Myles G, Radacsi N, Mo X. Recent advancements on three-dimensional electrospun nanofiber scaffolds for tissue engineering. *Adv Fiber Mater*. **2022**;*4*: 959.
68. Zhang YQ, Wang P, Shi QF, Ning X, Chen Z, Ramakrishna S, Zheng J, Long YZ. Advances in wet electrospinning: rich morphology and promising applications. *Adv Fiber Mater*. **2025**;*7*: 374.
69. Zong D, Zhang X, Yin X, Wang F, Yu J, Zhang S, Ding B. Electrospun fibrous sponges: principle, fabrication, and applications. *Adv Fiber Mater*. **2022**;*4*: 1434.
70. Song J, Lin X, Ee LY, Li SFY, Huang M. A review on electrospinning as versatile supports for diverse nanofibers and their applications in environmental sensing. *Adv Fiber Mater*. **2023**;*5*: 429.
71. Kong DH, Guo W, Zhao Y, Zhao Y. Electrospun multiscale structured nanofibers for lithium-based batteries. *Adv Energy Mater*. **2025**;*15*: 3983.
72. Yao S, Ramakrishna S, Chen G. Recent advances in metal–organic frameworks based on electrospinning for energy storage. *Adv Fiber Mater*. **2023**;*5*: 1592.
73. Dumitriu RP, Stoleru E, Rosnes JT, Sharmin N, Doroftei F, Brebu M. Rheological properties influence on the electrospinning of caseinate for loading with antioxidant rosemary extract. *Food Hydrocolloids*. **2024**;*151*: 109883.
74. Xue J, Wu T, Dai Y, Xia Y. Electrospinning and electrospun nanofibers: methods, materials, and applications. *Chem Rev*. **2019**;*16*: 5298.

75. Dong S, Maciejewska BM, Schofield RM, Hawkins N, Siviour CR, Grobert N. Electrospinning nonspinnable sols to ceramic fibers and springs. *ACS Nano*. **2024**;*18*: 13538.
76. Wen Y, Kok MDR, Tafoya JPV, Sobrido ABJ, Bell E, Gostick JT, Herou S, Schlee P, Titirici MM, Brett DJL, Shearing PR, Jervis R. Electrospinning as a route to advanced carbon fibre materials for selected low-temperature electrochemical devices: a review. *J Energy Chem*. **2021**;*59*: 492.
77. Wang P, Liu JH, Cui W, Li X, Li Z, Wan Y, Zhang J, Long YZ. Electrospinning techniques for inorganic–organic composite electrolytes of all-solid-state lithium metal batteries: a brief review. *J Mater Chem A*. **2023**;*11*: 16539.
78. Wang Y, Li N, Liu H, Shi J, Li Y, Wu X, Wang Z, Huang C, Chen K, Zhang D, Wu T, Li P, Liu C, Mi L. Zincophilic-hydrophobic" PAN/PMMA nanofiber membrane toward high-rate dendrite-free Zn anode. *Adv Fiber Mater*. **2023**;*5*: 2002.
79. Wu S, Tang F, Zhang K, Zhang L, Huang F. Synergistic long- and short-range sodium-ion transport pathways for enhanced low-temperature performance in ceramic-dee-polymer electrolytes. *Adv Funct Mater*. **2025**;*35*: 202501107.
80. Gou J, Cui K, Wang S, Zhang Z, Huang J, Wang H. An anisotropic strategy for developing polymer electrolytes endowing lithium metal batteries with electrochemo-mechanically stable interface. *Nat Commun*. **2025**;*16*: 58916.
81. Hwang SH, Song JY, Ryu HI, Oh JH, Lee S, Lee D, Park DY, Park SM. Adaptive electrospinning system based on reinforcement learning for uniform-thickness nanofiber air filters. *Adv Fiber Mater*. **2023**;*5*: 617.
82. Song JY, Kim S, Park J, Park SM. Highly efficient, dual-functional self-assembled electrospun nanofiber filters for simultaneous pm removal and on-site eye-readable formaldehyde sensing. *Adv Fiber Mater*. **2023**;*5*: 1088.
83. Gupta S, Sohail T, Checa M, Rohewal SS, Toomey MD, Kanbargi N, Damron JT, Collins L, Kearney LT, Naskar AK, Bowland CC. Enhancing composite toughness through hierarchical interphase formation. *Adv Sci*. **2024**;*11*: 202305642.
84. Lee JW, Na JH, Lee S, Kim S, Ryu HS, Kim K, Jang H, Park SK, Lim HD. Atomic-scale surface design for tailored nucleation in stable multivalent metal anodes. *J Mater Chem A*. **2025**;*5*: 6095.
85. Huang X, Zhao F, Teng Z, Li Y, Zhang C, Liu X, Li S, Xie F. Electrospinning of emulsions stabilized by octenylsuccinylated starch and pullulan. *Food Hydrocolloids*. **2025**;*158*: 110482.
86. Li L, Liu X, Wang G, Liu Y, Kang W, Deng N, Zhuang X, Zhou X. Research progress of ultrafine alumina fiber prepared by Sol-Gel method: a review. *Chem Eng J*. **2021**;*421*: 127744.
87. Qi X, Li Y, Zhang S, Li X, Wang X, Jiang H, Wu X, Ruan X, Jiang X, He G, Tu J. Nanofiber connected metal organic frameworks adsorption membrane to enhance Li^+ conduction and alleviate interfacial side reaction for solid electrolyte. *Chem Eng J*. **2024**;*501*: 157701.
88. Duan S, Qian L, Zheng Y, Zhu Y, Liu X, Dong L, Yan W, Zhang J. Mechanisms of the accelerated Li^+ conduction in MOF-based solid-state polymer electrolytes for all-solid-state lithium metal batteries. *Adv Mater*. **2024**;*36*: 2314120.
89. Yu W, Deng N, Feng Y, Feng X, Xiang H, Gao L, Cheng B, Kang W, Zhang K. Understanding multi-scale ion-transport in solid-state lithium batteries. *eScience*. **2025**;*5*: 100278.
90. Shen K, Yao X, Song H, Shi W, Zheng C, Hong X, Yan Y, Liu X, Zhu L, An Y, Song T, Shafqat MB, Ma C, Zheng L, Gao P, Liu Y, Safari M, Zhao Y, Pang Q. All-solid-state batteries stabilized with electro-mechano-mediated phosphorus anodes. *Energy Environ Sci*. **2025**;*18*:7568.
91. Ma Y, Zhang R, Wang L, Wu J, Chen B, Yu Y, Li L, He F, Shi C, Zhao N, He C, Wong AB. Self-healing polymer-based electrolyte induced by amorphous three-dimensional carbon for high-performance solid-state Li metal batteries. *Energy Storage Mater*. **2023**;*61*: 102893.
92. Chen Y, Feng Y, Ren Y, Huang K, Han S. Recent advances in high-entropy solid electrolytes for all-solid-state lithium batteries. *EnergyChem*. **2025**;*7*: 100157.
93. Li Z, Wang S, Shi J, Liu Y, Zheng S, Zou H, Chen Y, Kuang W, Ding K, Chen L, Lan Yq, Cai YP, Zheng Q. A 3D interconnected metal-organic framework-derived solid-state electrolyte for dendrite-free lithium metal battery. *Energy Storage Mater*. **2022**;*47*:262.
94. Li J, Xie F, Pang W, Liang Q, Yang X, Zhang L. Regulate transportation of ions and polysulfides in all-solid-state Li-S batteries using ordered-MOF composite solid electrolyte. *Sci Adv*. **2024**;*10*: 3925.
95. Razzaq AA, Yuan X, Chen Y, Hu J, Mu Q, Ma Y, Zhao X, Miao L, Ahn JH, Peng Y, Deng Z. Anchoring MOF-derived CoS_2 on sulfurized polyacrylonitrile nanofibers for high areal capacity lithium–sulfur batteries. *J Mater Chem A*. **2019**;*8*:1298.
96. Xu L, Yao M, Du L, Chen Y, Wei Y, Yuan D, Wu H, Zhang H, Zhang Y, Wang G. Accelerating lithium ion conduction via activated interfacial dipole layer for long-life and high-voltage solid-state lithium-metal battery. *J Energy Chem*. **2025**;*108*:92.
97. Xu M, Liang S, Shi H, Miao J, Tian F, Cui W, Shao R, Xu Z. High-strength MOF-based polymer electrolytes with uniform ionic flow for lithium dendrite suppression. *Small*. **2024**;*20*: e06007.
98. Ma Y, Qiu Y, Yang K, Lv S, Li Y, An X, Xiao G, Han Z, Ma Y, Chen L, Zhang D, Lv W, Tian Y, Hou T, Liu M, Zhou Z, Kang F, He YB. Competitive Li-ion coordination for constructing a three-dimensional transport network to achieve ultra-high ionic conductivity of a composite solid-state electrolyte. *Energy Environ Sci*. **2024**;*17*: e03134.
99. Liu X, Liang Q, Chen L, Tang J, Liu J, Tang M, Wang Z. PEO-based solid-state electrolytes reinforced by high strength, interconnected MOF networks. *ACS Appl Energy Mater*. **2023**;*6*:4881.
100. Wang L, Dong L, Wang Z, Shangguan E, Li J, Li L, Gao S, Deng N. Engineering 3D interpenetrated ZIF-8 network in poly(ethylene oxide) composite electrolyte for fast lithium-ion conduction and effective lithium-dendrite inhibition. *ACS Sustain Chem Eng*. **2023**;*11*:9337.
101. Ma X, Sun N, Li Z, Tong M, Ding Q, Wang Z, Bai L, Dong L, Liu Y. Highly flexible and self-standing covalent organic framework-metal-organic framework (COF-MOF) composite crystalline porous material (CPM) membrane for molecular separation. *Adv Funct Mater*. **2024**;*34*: 12203.
102. Gao J, Chai Y, Ni J, Zeng Y, Zhang G, Liu X, Ning D, Jin X, Zhao H, Zhou D, Gao R, Wu W, Wang J, Li Y. Fabrication of flexible polymer-MOF composite electrolyte for solid-state lithium metal batteries with high rate performance. *Chem Eng J*. **2025**;*512*: 162738.
103. Chai Y, Gao J, Yang L, Wu W, Ning D, Chen Z, Huang W, Zhang G, Gao R, Zhou D, Wang J, Huang SM, Li Y. In situ coordinated MOF-polymer composite electrolyte for solid-state lithium metal batteries with exceptional high-rate performance. *Small*. **2025**;*12*: 202412494.
104. Fan W, Huang Y, Yu M, She K, Gou J, Zhang Z. Designing metal-organic framework fiber network reinforced polymer electrolytes to provide continuous ion transport in solid state lithium metal batteries. *Nano Res*. **2023**;*17*: 12274.
105. Li M, Dou Y, Zhou Z, Li Z, Pan K, Zhang Z, Zhou Z. Innovative MOF linker engineering in PVDF-HFP gel electrolyte matrix for solid-state lithium-oxygen batteries. *Chem Eng J*. **2025**;*516*: 164013.

106. Chai Y, Ning D, Zhou D, Gao J, Ni J, Zhang G, Gao R, Wu W, Wang J, Li Y. Construction of flexible asymmetric composite polymer electrolytes for high-voltage lithium metal batteries with superior performance. *Nano Energy*. **2024**;*130*: 110160.
107. Tan E, Peng W, Li Q, Wang D, Li X, Duan J, Guo H, Yan G, Wang J, Wang Z. Synergy of PVDF-HFP and ZIF-8 promotes PEO electrolyte towards all-solid-state lithium battery. *Electrochim Acta*. **2023**;*473*: 143469.
108. Deng N, Wang L, Feng Y, Liu M, Li Q, Wang G, Zhang L, Kang W, Cheng B, Liu Y. Co-based and Cu-based MOFs modified separators to strengthen the kinetics of redox reaction and inhibit lithium-dendrite for long-life lithium-sulfur batteries. *Chem Eng J*. **2020**;*388*: 124241.
109. Yu W, Shen L, Lu X, Han J, Geng N, Lai C, Xu Q, Peng Y, Min Y, Lu Y. Novel composite separators based on heterometallic metal-organic frameworks improve the performance of lithium-ion batteries. *Adv Energy Mater*. **2023**;*13*: 202204055.
110. Luo S, Deng N, Wang H, Zeng Q, Li Y, Kang W, Cheng B. Facilitating Li^+ conduction channels and suppressing lithium dendrites by introducing Zn-based MOFs in composite electrolyte membrane with excellent thermal stability for solid-state lithium metal batteries. *Chem Eng J*. **2023**;*474*: 145683.
111. Lan F, Zhao H, Jiang Y, Jin C, Zhao G, Li L. A thermomechanically stable nanofiber separator with multiscale MOF networks towards high-efficiency ion transport. *J Mater Chem A*. **2025**;*13*:7357.
112. Zheng Y, Yao Y, Ou J, Li M, Luo D, Dou H, Li Z, Amine K, Yu A, Chen Z. A review of composite solid-state electrolytes for lithium batteries: fundamentals, key materials and advanced structures. *Chem Soc Rev*. **2020**;*49*:8790.
113. Liu S, Liu W, Ba D, Zhao Y, Ye Y, Li Y, Liu J. Filler-integrated composite polymer electrolyte for solid-state lithium batteries. *Adv Mater*. **2023**;*35*: 2110423.
114. Chen K, Lu M, Li X, Yang S, Bagherzadeh R, Lai F, Zhang C, Miao YE, Liu T. Vertically directed ion transport at the molecular scale in composite solid electrolytes enabled by nanofiber-confined alignment of single-crystal mof tubes. *ACS Appl Mater Interfaces*. **2025**;*17*:39064.
115. Shan Y, Li L, Chen X, Fan S, Yang H, Jiang Y. Gentle haulers of lithium-ion–nanomolybdenum carbide fillers in solid polymer electrolyte. *ACS Energy Lett*. **2022**;*7*:2289.
116. Yu X, Zhao L, Li Y, Jin Y, Politis DJ, Liu H, Wang H, Liu M, He Y-B, Wang L. Weakening ionic coordination for high ionic conductivity composite solid electrolytes. *ACS Energy Lett*. **2024**;*9*:2109.
117. Zhou S, Zhong S, Dong Y, Liu Z, Dong L, Yuan B, Xie H, Liu Y, Qiao L, Han J, He W. Composition and structure design of poly(vinylidene fluoride)-based solid polymer electrolytes for lithium batteries. *Adv Funct Mater*. **2023**;*33*: 14432.
118. Xia X, Zhang ZQ, Wen Q, Li PY, Le DH, Wang ZY, Dong PP, Ren GD, Zheng JC. Metal-organic-framework-based solid-state electrolytes for high-performance lithium metal batteries: recent advances and prospects. *Chin Chem Lett*. **2025**;*7*: 111653.
119. Wang L, Wang Z, Su Z, Fang B, Mo R. Interface-engineered strategy on metal-organic framework to chemical stabilize PVDF-HFP as self-healing high-voltage quasi-solid-state electrolyte. *Small*. **2025**;*21*: e08318.
120. Zhang S, Li Y, Liu J, Yang X, Qi X, Li X, He G. Metal organic frameworks intensify lithium ion conduction and SEI formation inlayed in solid electrolyte facing with lithium metal anode. *Chem Eng J*. **2025**;*510*: 161669.
121. Zheng Y, Yang N, Duan S, Li Z, Gao R, Zhu Y, Wang H, Zhang T, Li G, Luo D, Yang L, Wang D, Yan W, Zhang J, Chen Z. Dual-enhanced charge transfer through prelithiation strategy in polymer electrolyte enables robust LiF-rich SEI for ultralong-life all-solid-state batteries. *Adv Funct Mater*. **2025**;*10*: e11011.
122. Sun M, Li J, Yuan H, Zeng X, Lan J, Yu Y, Yang X. Fast Li^+ transport pathways of quasi-solid-state electrolyte constructed by 3D MOF composite nanofibrous network for dendrite- free lithium metal battery. *Mater Today Energy*. **2022**;*29*: 101117.
123. Zheng Y, Yang N, Gao R, Li Z, Dou H, Li G, Qian L, Deng Y, Liang J, Yang L, Liu Y, Ma Q, Luo D, Zhu N, Li K, Wang X, Chen Z. "Tree-trunk" design for flexible quasi-solid-state electrolytes with hierarchical ion-channels enabling ultralong-life lithium-metal batteries. *Adv Mater*. **2022**;*34*: 2203417.
124. Chai Y, Gao J, Yang L, Wu W, Ning D, Chen Z, Huang W, Zhang G, Gao R, Zhou D, Wang J, Huang SM, Li Y. In situ coordinated MOF-Polymer composite electrolyte for solid-state lithium metal batteries with exceptional high-rate performance. *Small*. **2025**;*12*: 2412494.
125. Guo J, Feng F, Jiang X, Wang R, Chu D, Ren Y, Chen F, He P, Ma ZF, Chen S, Liu T. Boosting selective Na^+ migration kinetics in structuring composite polymer electrolyte realizes ultrastable all-solid-state sodium batteries. *Adv Funct Mater*. **2024**;*34*: 2313496.
126. Yang M, Feng F, Ren Y, Chen S, Chen F, Chu D, Guo J, Shi Z, Cai T, Zhang W, Ma ZF, Chen S, Liu T. Coupling anion-capturer with polymer chains in fireproof gel polymer electrolyte enables dendrite-free sodium metal batteries. *Adv Funct Mater*. **2023**;*33*: 2305383.
127. Yuan W, Ding M, Weng J, Xue T, Xie M, Zhang P, Mu J, Zhou P. Composite electrolyte membrane with continuous Na plus transport for high-performance quasi-solid-state sodium batteries. *Chem Eng J*. **2025**;*514*: 163142.
128. Tian W, Lin G, Yuan S, Jin T, Wang Q, Jiao L. Competitive coordination and dual interphase regulation of MOF-modified solid-state polymer electrolytes for high-performance sodium metal batteries. *Angew Chem Int Ed*. **2025**;*64*: 202423075.